UNIVERSITY OF CALIFORNIA,
IRVINE

Mode Coupling and Degeneracy Condition in Multilayer Waveguide Structure with Grating

THESIS

submitted in partial satisfaction of the requirements
for the degree of

MASTER OF SCIENCE

in Electrical Engineering

by

Puxi Zhou

Thesis Committee:
Professor Filippo Capolino, Chair
Professor Michael M. Green
Associate Professor Ozdal Boyraz

2018

DEDICATION

To

my parents and my girlfriend

TABLE OF CONTENTS

LIST OF FIGURES

ACKNOWLEDGMENTS

I would like to express the deepest appreciation to my committee chair, Professor Filippo Capolino, who has the attitude and the substance of a genius: he continually and convincingly conveyed a spirit of adventure in regard to research and scholarship, and an excitement in regard to teaching. Without his guidance and persistent help this thesis would not have been possible. I would like to thank my committee members, Professor Michael M. Green and Professor Ozdal Boyraz, for their kind help.

In addition, a thank you to Professor Tianrui Zhai at Beijing University of Technology, who introduced me to the topic of distributed feedback laser. Thank you to Professor Henry P. Lee, who provided me with a lot of guidance for my career.

I thank my colleagues who were involved in this research, Mohamed Nada, Ahmed F. Abdelshafy, and Tarek Mealy for helping me with solving various problems. Thank you to my friend Muhannad Alshetaiwi, who always supported me. I also thank my labmates, Hamidreza Kazemi, Ahmed Almutawa, Mohammad Kamandi, Mahsa Darvichzade, Dmitry Oshmarin, and Farshad Yazdi.

I dedicate this work to my parents and my girlfriend whose love and support gave me the strength to pursue my passion and thrive.

ABSTRACT OF THE THESIS

Mode Coupling and Degeneracy Condition in Multilayer Waveguide Structure with Grating

By

Puxi Zhou

Master of Science in Electrical Engineering

University of California, Irvine, 2018

Professor Filippo Capolino, Chair

Intra mode coupling effects and degeneracy conditions are thoroughly investigated in the scenario of multilayer waveguide structures with grating. Propagating modes in uniform slab waveguides are exactly solved by a transfer matrix method, with modes' profiles and dispersion characteristics illustrated. Modes coupling phenomena in parallel slab waveguides is studied through inspecting the spatial evolution of single mode's profile as well as superimposed field distribution. Floquet-Bloch analysis is implemented to accurately solve the modes in single slab waveguides with periodic grating. Dispersion relations are obtained for both propagating modes and evanescent modes in the structure, where second order mode degeneracy is demonstrated at the regular photonic band edge. Through examining the fields' distribution and spatial evolution, the fundamental harmonic and the -1st Floquet harmonic are illustrated. Finally, coupled mode theory is implemented to support better understandings of the various coupling phenomena. Moreover, a coupled mode model is developed for the parallel slab waveguides with a grating structure in between, and the existence of the degenerate band edge in such stricture is qualitatively demonstrated.

Chapter 1

Introduction

1.1 Mode Degeneracy in Optical Frequency

Mode degeneracies at the photonic band edges have been demonstrated in various photonic devices, such as distributed feedback (DFB) lasers, distributed Bragg reflectors (DBR), coupled resonators optical waveguides, degenerate band edge resonators, etc. [1]–[5]. According to the number of modes that are degenerated at the photonic band edges, the photonic band edges can be classified as regular band edges (RBE) or degenerate band edges (DBE). Specifically, at the regular band edges, there are two modes coalescing to form a degenerate mode, while four modes are involved into the mode degeneracy at the degenerate band edges. Operating at photonic band edges can lead to several promising characteristics of the photonic devices, such as frequency stability and selectivity, giant gain enhancement, and high quality factors [4], [6]–[8]. Furthermore, the photonic devices operating at the DBE have been illustrated to possess much better performance than those operating at the RBE [4], [7], [8]

The modes coupling effects play a critical role in forming photonic band edges. Regular band edges have been found in multiple periodic photonic structures such as the DFB laser cavities and the distributed Bragg reflectors. In those cases, photonic band gaps and regular band edges are formed thanks to the contra-directional coupling effects between the two oppositely propagating modes. Degenerate band edges have been demonstrated in optical

fibers [9], [10], coupled photonic crystal waveguide [5], [11], and coupled resonator optical waveguides [4]. To achieve those degenerate band edges, the supported modes in those structures have been carefully determined, and the related modes coupling effects have been rigorously analyzed as well as elaborately controlled.

1.2 Motivation

Integrated photonic devices and systems have attracted extensive attention over the years for its great application potentials in data communication infrastructures, novel computing systems, biomedical research platforms, etc.[12]–[14]. Engineering the modes behavior inside the photonic structures is an important way to design and achieve high-performance photonic devices, of which the photonic devices operating at the photonic band edges is a good example. Among the diverse photonic structures, the multilayer waveguide structures with grating appeals our particular interest because on one hand, this type of structures constitute key elements of various photonic devices [15]–[17]. On the other hand, the degenerate band edge has not been demonstrated in this kind of geometry.

In this report, we systematically study the modes behavior in the multilayer waveguide structures with grating, which includes the dispersion characteristics, mode profiles, field evolutions, and mode couplings. Specifically, understanding the modes behavior in the uniform (non-grating) multilayer structures is the prerequisite to analyze the structures with grating. Therefore, we first study the single and coupled slab waveguides that can be formed in uniform multilayer systems. Then, the single slab waveguide with periodic grating is analyzed, which has been demonstrated to possess regular band edges. The modes

behavior is mainly discussed in terms of the degeneracy conditions as well as the coupling effects. Based on these analysis, we finally propose a coupled slab waveguides structure with a periodic structure in between and study the degeneracy conditions of the degenerate band edges in the scope of coupled mode theory.

1.3 Analyzing Methods

Multilayer waveguide structures with/out grating have been subjects of numerous theoretical investigations [18], [19], where different analyzing methods were implemented. In this report, we adopted three methods, which are transfer matrix method, Floquet-Bloch analysis, and coupled mode theory.

The transfer matrix method is first implemented to provide exact solutions of the modes supported in the uniform multilayer waveguide structures. The transfer matrices are obtained through applying boundary conditions at each interface between the layers. Using the transfer matrix method, not only the dispersion characteristic, but also the mode profile can be obtained and analyzed for each supported mode.

Floquet-Bloch analysis is a powerful tool to obtain the exact solutions of the fields in the photonic periodic structures. In this report, it is implemented to analyze both single and coupled slab waveguides with a periodic grating structure. Floquet-Bloch method maintains higher accuracy compared with other techniques for analyzing the periodic structures, because the fields in the periodic structures can be thoroughly described according to the Floquet-Bloch theory. Moreover, not only propagating modes, but also evanescent modes can be exactly solved through the Floquet-Bloch method.

Coupled mode theory is implemented to support better understandings of the diverse coupling phenomenon. Through determining the coupled mode equation for each scenario of interest, the dispersion relations of the supported modes can be obtained by solving eigenvalue problems. In this way, we can have a qualitative analysis of the mode behaviors in the structure.

Overall, this report is organized in the following manner. In chapter 2, multilayer waveguide structure is analyzed using the transfer matrix method as well as the coupled mode theory. The dispersion characteristics, mode profiles, as well as modes coupling effects are studied in this scenario. In chapter 3 and 4, single slab waveguide with a periodic grating is investigated through the two methods respectively: the Floquet-Bloch analysis based on Maxwell equations and the coupled mode theory that is a physically-incisive method to understand wave phenomena though not strictly related to a precise structure. Modes behavior is fully analyzed in terms of mode degeneracy and modes coupling. In Chapter 4, we illustrate the dispersion characteristic of a coupled periodic multilayer structure based on a coupled mode model. Degenerate band edge conditions are qualitatively discussed. Finally, in chapter 5, a summary of this report is provided, followed by the future work proposed.

Chapter 2

Multilayer Waveguide Structure

2.1 Introduction

Multilayer waveguide structures have been widely adopted in contemporary integrated photonic devices and systems [14], [20], [21], of which the key elements are known as slab or planar optical waveguides. In his chapter, single and coupled optical slab waveguides are analyzed using a transfer matrix method [18], [22]. The dispersion characteristics of propagating modes with TE polarization are obtained by implementing the transfer matrix method, followed by illustrating the mode profiles. This method also can be used to solve TM modes with modifications to relevant formulas, which is not included here for the sake of brevity. Several phenomenon related to the results are also discussed. Finally, coupled mode analysis is implemented to facilitate a better understanding of the coupled optical waveguides.

2.2 Transfer Matrix Method

This section introduces the transfer matrix method [18], [22], which is used to obtain the dispersion characteristic and field distributions in multilayer waveguide structures. A basic configuration of a multilayer system is shown in Fig. 2. 1, where the layers are ordered along the x-direction and x_i is the interface between the ith and $(i+1)$th layers. Each layer consists of one type of isotropic and homogeneous dielectric media and the relative dielectric

constant of the ith layer is denoted as ε_i. Both superstrate (layer 1) and substrate (layer s) are assumed to be semi-infinite regions.

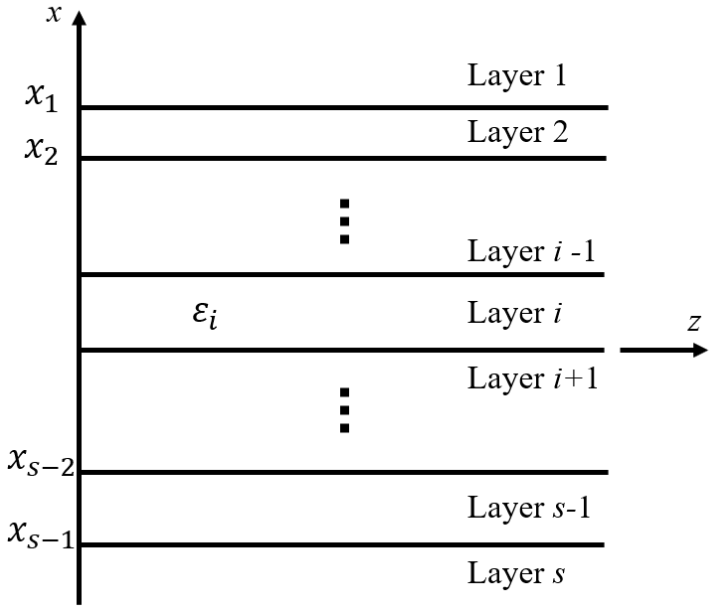

Fig. 2. 1. Basic schematic of a multilayer structure. Layers are ordered along the x-axis, layer 1 and s are superstrate and substrate respectively, which are assumed to be semi-infinite regions. $x = x_i$ is the interface between the i^{th} and the $(i+1)^{\text{th}}$ layer. Each layer consists of one type of isotropic and homogeneous material, and ε_i is the relative dielectric constant of ith layer. The structure is assumed to be infinite along the y-direction.

Consider a monochromatic plane wave that travels along the z-direction with the time dependence of $e^{j\omega t}$. For TE polarization, the electric and magnetic fields can be expressed as $\vec{E} = \hat{y}E_y$ and $\vec{H} = \hat{x}H_x + \hat{z}H_z$, where all the field components are constant along the y-direction (see Appendix A) as the structure is assumed to be infinite along the y-direction. Since the electric field has only one component, we can apply the scalar wave equation to describe the wave in each layer as [22]

$$\frac{\partial^2}{\partial x^2} E_y^{(i)}(x) + (\varepsilon_i k_0^2 - k_z^2) E_y^{(i)}(x) = 0 \tag{2.1}$$

where k_0 and k_z are the free-space wavenumber and the propagation constant along z, respectively, while $E_y^{(i)}(x)$ denotes the electric field in the ith layer. We further define the

transverse wavenumber (orthogonal to the layers) for the ith layer as

$$k_x^{(i)} = \pm\sqrt{\varepsilon_i k_0^2 - k_z^2}. \tag{2.2}$$

The solutions of the wave equation (2.1) are in the form

$$E_y^{(i)}(x) = \begin{cases} b^{(1)} \exp\left(-jk_x^{(1)}|x|\right) & i = 1 \\ a^{(i)} \exp\left(jk_x^{(i)}x\right) + b^{(i)} \exp\left(-jk_x^{(i)}x\right) & i = 2{\sim}s-1 \\ a^{(s)} \exp\left(jk_x^{(s)}|x|\right) & i = s \end{cases} \tag{2.3}$$

where $a^{(i)}$ and $b^{(i)}$ are defined as amplitude coefficients for the ith layer. Since there is no field component propagating toward the structure from the superstrate or substrate, we have $a^{(1)} = b^{(s)} = 0$. To make the solution have a physical meaning, it is critical to appropriately determine the proper branch choice of the transverse wavenumber in the open half spaces (i.e. signs of $k_x^{(1)}$and $k_x^{(s)}$). In order to make the proper choice, let's consider the limit when $x \to \pm\infty$, $E_y^{(1)}(x)$ and $E_y^{(s)}(x)$ are supposed to be zero respectively. Accordingly, the transverse field should be exponentially decaying away from the structure as

$$Im\left(k_x^{(1)}\right) < 0 \text{ and } Im\left(k_x^{(s)}\right) < 0. \tag{2.4}$$

At a certain frequency, to find a physical mode is to find its propagation constant as well as its transverse wavenumber. The dispersion characteristics are obtained by solving for the existing propagation constants for frequencies of interest. The physical modes in a multilayer structure can be found by solving the wave equations and applying the proper boundary conditions at each interface. The boundary conditions for TE modes are applied by enforcing continuity of both $E_{y-}(x_i) = E_{y+}(x_i)$ and $\frac{\partial E_{y-}(x_i)}{\partial x} = \frac{\partial E_{y+}(x_i)}{\partial x}$ at each interface

$x = x_i$ (see Appendix A). Then, if we define the amplitude coefficients vector for the ith layer as $\underline{C}^{(i)} = \begin{pmatrix} a^{(i)} \\ b^{(i)} \end{pmatrix}$, and take advantage of (2.3), we can express the boundary conditions as

$$\underline{\underline{T}}^{(i)}\underline{C}^{(i)} = \underline{\underline{M}}^{(i+1)}\underline{C}^{(i+1)} \tag{2.5}$$

where $\underline{\underline{T}}^{(i)}$ and $\underline{\underline{M}}^{(i+1)}$ are the transfer matrices associated to the interface $x = x_i$, which are given for TE modes as [22]

$$\underline{\underline{T}}^{(i)} = \begin{pmatrix} \exp\left(jk_x^{(i)}x_i\right) & \exp\left(-jk_x^{(i)}x_i\right) \\ jk_x^{(i)}\exp\left(jk_x^{(i)}x_i\right) & -jk_x^{(i)}\exp\left(-jk_x^{(i)}x_i\right) \end{pmatrix} \tag{2.6.a}$$

$$\underline{\underline{M}}^{(i+1)} = \begin{pmatrix} \exp\left(jk_x^{(i+1)}x_i\right) & \exp\left(-jk_x^{(i+1)}x_i\right) \\ jk_x^{(i+1)}\exp\left(jk_x^{(i+1)}x_i\right) & -jk_x^{(i+1)}\exp\left(-jk_x^{(i+1)}x_i\right) \end{pmatrix}. \tag{2.6.b}$$

The only difference between $\underline{\underline{T}}^{(i)}$ and $\underline{\underline{M}}^{(i+1)}$ is the transverse wavenumbers they applied. Therefore, the amplitude coefficients vector for the ith layer can be recursively related to that for the superstrate $\underline{C}^{(1)}$ through

$$\begin{aligned} \underline{C}^{(i)} &= \left(\underline{\underline{M}}^{(i)}\right)^{-1}\underline{\underline{T}}^{(i-1)}\underline{C}^{(i-1)} \\ &= \underline{\underline{S}}^{(i-1)}\underline{C}^{(i-1)} = \underline{\underline{S}}^{(i-1)} \cdots \underline{\underline{S}}^{(1)}\underline{C}^{(1)} = \underline{\underline{S}}\underline{C}^{(1)} \end{aligned} \tag{2.7}$$

where $\underline{\underline{S}}$ is the transfer matrix that relate $\underline{C}^{(i)}$ to $\underline{C}^{(1)}$. Similarly, $\underline{C}^{(i)}$ can be recursively related to the amplitude coefficients vector for the substrate $\underline{C}^{(s)}$ as

$$\begin{aligned} \underline{C}^{(i)} &= \left(\underline{\underline{T}}^{(i)}\right)^{-1}\underline{\underline{M}}^{(i+1)}\underline{C}^{(i+1)} \\ &= \underline{\underline{R}}^{(i+1)}\underline{C}^{(i+1)} = \underline{\underline{R}}^{(i+1)} \cdots \underline{\underline{R}}^{(s)}\underline{C}^{(s)} = \underline{\underline{R}}\underline{C}^{(s)} \end{aligned} \tag{2.8}$$

where $\underline{\underline{R}}$ is the transfer matrix that relate $\underline{C}^{(i)}$ to $\underline{C}^{(s)}$. Therefore, the characteristic equation for our system can be easily obtained by equating (2.7) and (2.8), i.e. $\underline{\underline{R}}\underline{C}^{(s)} - \underline{\underline{S}}\underline{C}^{(1)} = 0$. This characteristic equation can be recanted as following, given that $a^{(1)} = b^{(s)} = 0$

$$\begin{pmatrix} r_{11} & -s_{12} \\ r_{21} & -s_{22} \end{pmatrix} \begin{pmatrix} a^{(s)} \\ b^{(1)} \end{pmatrix} = \underline{\underline{D}} \begin{pmatrix} a^{(s)} \\ b^{(1)} \end{pmatrix} = 0 \tag{2.9}$$

where r and s represents the matrix elements of $\underline{\underline{R}}$ and $\underline{\underline{S}}$ respectively, which are also functions of the propagation constant k_z, and $\underline{\underline{D}}$ is the coefficient matrix of the characteristic equation. The characteristic equation will have nontrivial solutions if

$$\det(\underline{\underline{D}}) = 0 \tag{2.10}$$

in other words, when the determinant of $\underline{\underline{D}}$ is zero. Solving (2.10) will provide the propagation constants of physical modes that exist in the system, and the corresponding transverse wavenumber in each layer can be calculated via (2.2). Meanwhile, based on the determined $\underline{\underline{D}}$, if we set a value of either $a^{(s)}$ or $b^{(1)}$, the other one can be easily calculated using the characteristic equation (2.9). Furthermore, the amplitude coefficients $a^{(i)}$ and $b^{(i)}$ for all intermediate layers can be obtained by applying the boundary conditions. Finally, the mode profile along the transverse direction can be obtained and inspected through applying all $a^{(i)}$, $b^{(i)}$ and $k_x^{(i)}$ to (2.3).

2.3 Single Slab Waveguide

In this section, the transfer matrix method is implemented to analyze the single slab optical waveguides. A basic geometry of such waveguide is shown in Fig. 2.2, where silicon is selected as the core layer material whereas silicon dioxide is selected as the cladding layer material. The core layer has a thickness of t, while both the cladding layers are assumed to be infinite half spaces. For the sake of simplicity, all the materials in our system are assumed to be non-dispersive, which means that their refractive indices are invariant with respect to

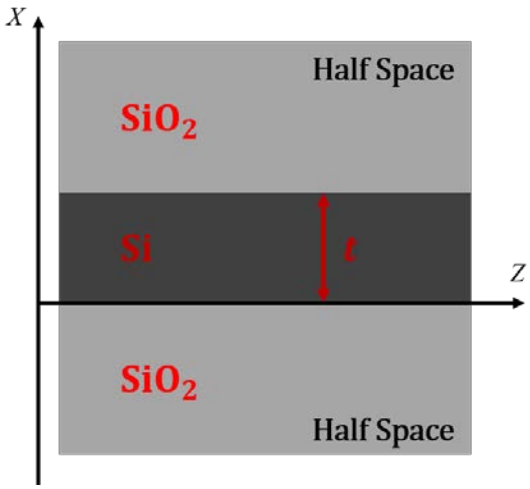

Fig. 2. 2. Geometry of a single slab optical waveguide. The materials for core layer and cladding layers are silicon and silicon dioxide respectively, whose refractive indices are $n_{\mathrm{Si}} = 3.48$ and $n_{\mathrm{SiO_2}} = 1.444$ respectively. The core layer has a thickness of *t,* whereas the cladding layers are assumed to be semi-infinite layers.

frequency, which is an excellent approximation for monochromatic signals.

The refractive indices adopted here for the silicon and silicon dioxide are $n_{\mathrm{Si}} = 3.48$ and $n_{\mathrm{SiO_2}} = 1.444$ respectively. These values are picked for a wavelength $\lambda_0 = 1550\mathrm{nm}$, where λ_0 is the wavelength in free space. Two waveguides are studies: waveguide 1 and waveguide 2. In the following we assume $t = 80\mathrm{nm}$ for waveguide 1 and $t = 350\mathrm{nm}$ for waveguide 2. Through solving (2.10) for the two geometries with different core thickness's, the dispersion characteristics are obtained for propagating modes with TE polarization. The $k - \omega$ dispersion diagrams are shown in Fig. 2.3.

In the dispersion diagrams, the center angular frequency ω_0 corresponds to the free-space wavelength 1550nm. For a propagating mode in lossless systems, its propagation constant k_z is a pure real number and is in the range between $n_{\mathrm{SiO_2}} k_0$ and $n_{\mathrm{Si}} k_0$ in this scenario. Therefore, in the dispersion diagrams, all points that represent the propagating modes are in the region defined by the two so-called light lines. The Si and SiO_2 light lines

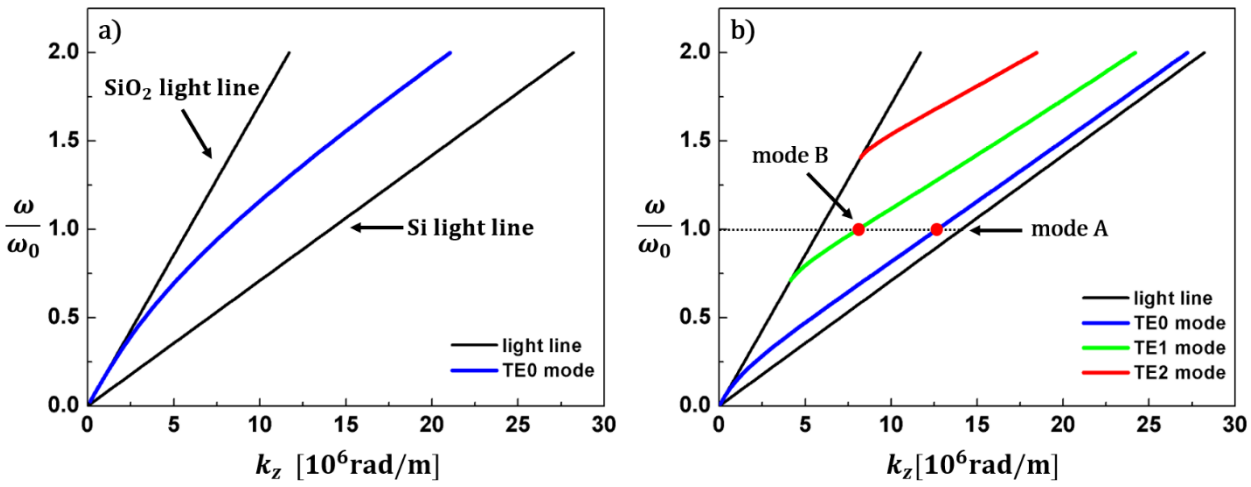

Fig. 2. 3. The *k*-*ω*, dispersion diagrams, for TE modes of a) waveguide 1, and b) waveguide 2. The black lines are light lines that define the region for propagating modes in the substrate and superstrate. The colored lines are dispersion curves for different order.

are given by $\omega = \frac{c}{n_{\mathrm{Si}}} k_0$ and $\omega = \frac{c}{n_{\mathrm{SiO_2}}} k_0$ respectively, where c denotes the speed of light in free space. It is worth noting that, waveguide 1 only supports the fundamental TE mode for the frequencies of interest. as shown in Fig. 2.3(a). On the other hand, Fig. 2.3(b) shows that, with a thicker core layer, multiple TE modes can be supported by waveguide 2 in the same range of interested frequencies. In addition, through comparing the two figures, it can be found that the dielectric slab waveguides support fundamental TE mode for all frequencies, while there are cutoff frequencies for higher order TE modes.

To provide deeper insight into the mode behavior, the mode profiles along the *x*-direction are plotted for modes A and B, which are labelled in Fig. 2.3(b) by red dots. The amplitude coefficients are calculated by solving (2.7) and (2.8) with the calculated propagation constant and the assumption that $b^{(1)} = 1$. The field distribution along the *x*-direction is calculated by inserting calculated propagation constant As shown in Fig. 2.4, modes A and B correspond to TE0 and TE1 mode i The refractive indices' profile is also plotted to illustrate the waveguide's geometry. From these figures, one can see that fields of

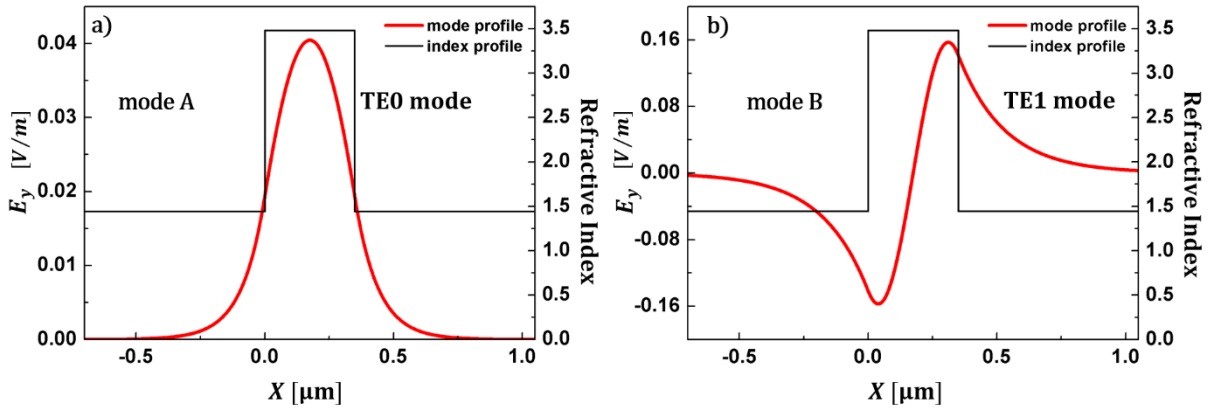

Fig. 2. 4. Field distribution and refractive index profile along the x-direction of a) mode A, and b) mode B that are marked in Fig. 2.3.

the propagating modes are confined in the core layer while decaying in the cladding layers. Moreover, the field distribution of TE0 mode is an even function over the transverse direction, by which it is known as a TE even mode. Similarly, TE1 mode is one of the TE odd modes as its field distribution is an odd function over the *x*-direction.

2.4 Coupled Slab Waveguide

In this section, we analyze coupled slab waveguide structures using the transfer matrix method. A typical geometry of the structure is shown in Fig. 2.5, where the materials of the two core layers are selected to be indium phosphide and silicon respectively. Silicon dioxide is the material of all the cladding layers. The InP and Si core layers have a thickness of t_1 and t_2 respectively, and the gap between them has a thickness of g. The refractive index of InP is set as $n_{\mathrm{InP}} = 3.167$, which corresponds to the free-space wavelength 1550nm.

Following the same procedure in section 2.3, the dispersion diagrams are plotted for

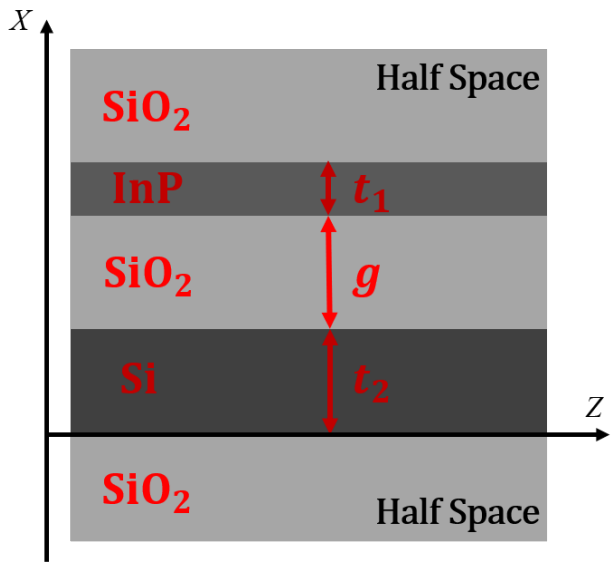

Fig. 2. 5. Geometry of a coupled slab optical waveguide structure. The cores layers consist of Si and InP respectively, and the cladding layers are made from SiO_2. The thicknesses of core layers are denoted as t_1 and t_2 respectively. The gap between the core layers has a thickness of g.

propagating TE modes in a coupled slab waveguide structure, which are shown in Fig. 2.6. The structure has $t_1 = 60\text{nm}$, $t_2 = 302\text{nm}$, and $g = 1000\text{nm}$. In Fig. 2.6, the blue curves represent propagating modes that have TE polarization, other labels and parameters have the same definitions as those in Fig. 2.3.

In Fig. 2.6(a), the new and most interesting feature is that two of the dispersion curves seems to "intersect" with each other near the center angular frequency, which is marked by a red ring. To study this feature, we zoom in on the marked part and display it in Fig. 2.6(b),where we can clearly see that instead of intersecting, the two curves "veer out" near the center angular frequency [23]. According to [18], [23] this phenomenon indicates that, in the veering region, the two modes with the same frequencies couple with each other. To gain a better understanding of this coupling phenomenon, we choose mode C and D at the center angular frequency ω_0 and plot their mode profiles along the x-direction, which are shown in Fig. 2.7.

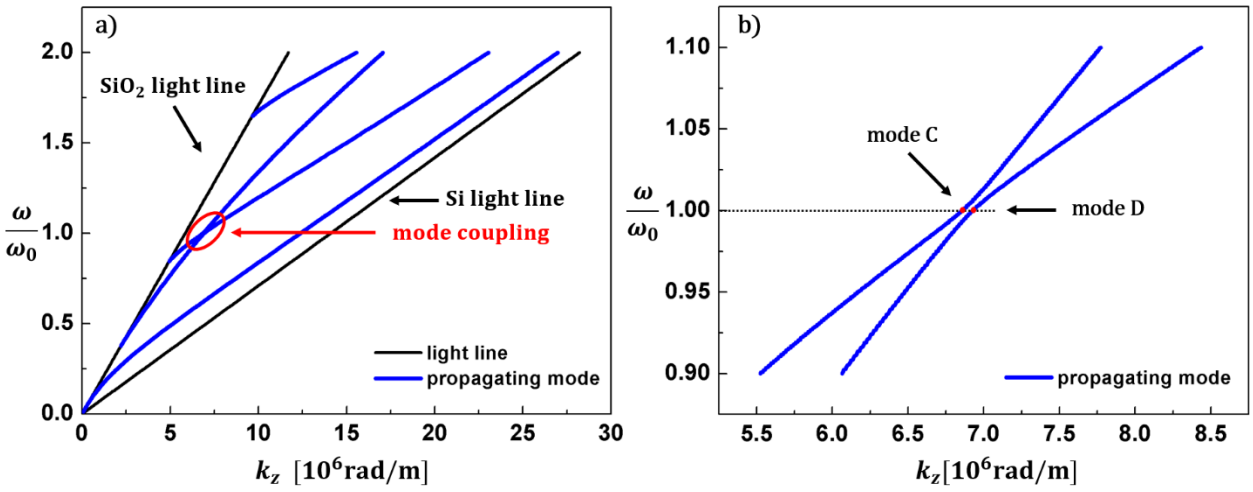

Fig. 2. 6. a) TE modes' dispersion diagram of a coupled slab waveguide structure with t_1=60nm, t_2=302nm, g=1000nm, b) zoom-in figure of the red-circled part in a). The black lines are light lines that define the region of propagating modes, whereas the blue lines are dispersion curves for distinct TE modes.

Before inspecting Fig. 2.7, based on Fig. 2.6 and the findings we obtained in section 2.3, we can infer that mode C corresponds to a TE1 mode of the silicon waveguide, and mode D corresponds to a TE0 mode of the InP waveguide. However, from Fig. 2.7, one can see that mode C and mode D do not possess the isolated TE1- and TE0-mode profile in Si and InP waveguides respectively. Instead, for mode C and mode D, their fields in the two core layers are both strong and correlated with each other. Moreover, their mode profiles are similar in

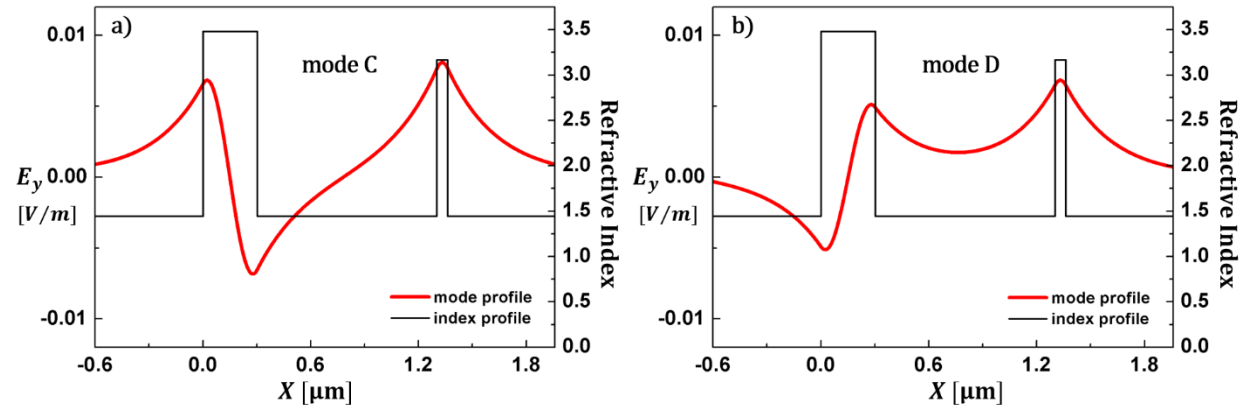

Fig. 2. 7. Mode and refractive index profiles along the x-direction of individual modes: a) mode C and b) mode D at ω_0 that are marked in Fig. 2.6.

the way that they both consist of a TE0-like field shape in InP layer and a TE1-like field shape in Si layer. All these phenomena indicate and illustrate the coupling effect between mode C and mode D at the center angular frequency.

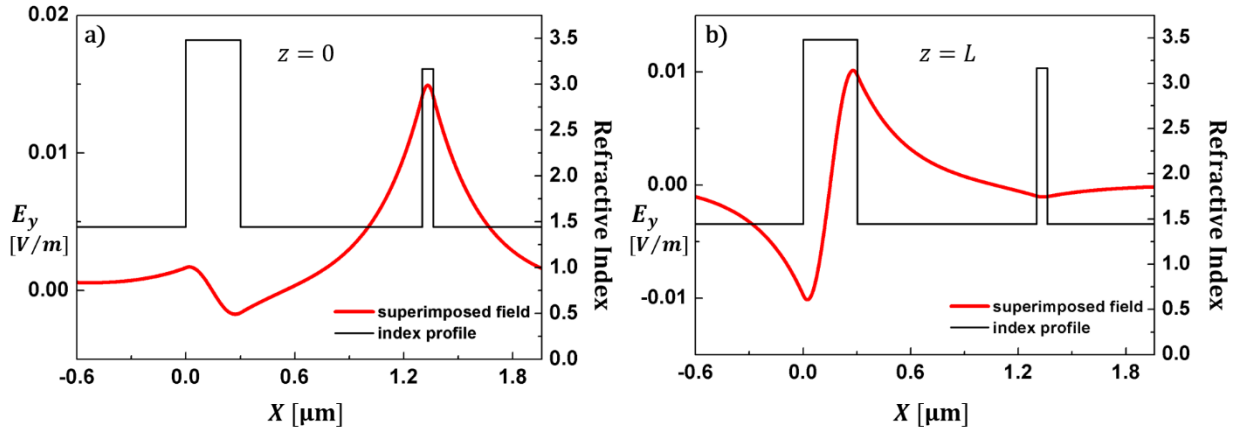

Fig. 2. 8. Superimposed field distribution of adding mode C and D, along with the refractive index profile along the x-direction at a) z = 0 and b) $z = L$.

Adding the profiles of the two modes provides their superimposed field distribution. Their superimposed field along the x-direction is shown in Fig. 2.8(a), from which we can see a TE0-like field distribution across all layers with a concentration at InP layer. It is worth noting that, the superimposed field distribution is not static, but it is evolving along the z-direction, and the result in Fig. 2.8(a) can be regarded as the superimposed field distribution at z = 0. The coupling effect between two propagating modes in two waveguides will lead to a transfer of power from one waveguide to the other along the propagating direction. The coupling length L is defined as the distance that maximum power exchanging is achieved between the two waveguides [22], [24]. The L can be calculated through

$$L = \frac{\pi}{|\beta_1 - \beta_2|} \tag{2.11}$$

where β_1 and β_2 are the propagation constant of the two coupled modes. Having calculated the L for mode C and D, we plot the superimposed field distribution at $z = L$ and display it in

Fig. 2.8(b). Comparing Fig. 2.8(a) and (b), we can easily find that the concentration of field totally shifts from the InP waveguide to the Si waveguide, which is consistent with the theoretical prediction.

2.5 Coupled Mode Analysis

In this section, we implement the well-known coupled mode theory [25]–[28] to support a better understanding of the coupling effect between two propagating modes. Specifically, we focus on the veering region in Fig. 2.6, in which the two modes with the same frequency will couple to each other. In the following, the technique we used is based on [29]. Consider a parallel slab waveguide structure which consists of waveguide a and waveguide b. We first treat each waveguide as an isolated waveguide, so that a TE wave that propagates along the z-direction in waveguide a can be generally described as

$$E_y^{(a)}(x,z) = E_y^{(a)}(x)a(z) \tag{2.12}$$

where $a(z)$ is the field distribution along the z-direction. The field evolution along the propagating direction can be described as: $\frac{\partial a(z)}{\partial z} = -j\beta_a a(z)$, where β_a is defined as the phase constant of that wave. Similar descriptions can be given for of a propagating mode with TE polarization in waveguide b if we define $b(z)$ and β_b as its field distribution and phase constant along the z-direction respectively. Then, we analyze the compound structure that has two parallel waveguides. In general, the total field in the structure can be expressed as a linear superposition of the single waveguide modes

$$E_y^{(tot)}(x,z) = E_y^{(a)}(x)a(z) + E_y^{(b)}(x)b(z) \tag{2.13}$$

where $E_y^{(tot)}$ denotes the total field in the structure. However, when the coupling effect between two propagating modes are considered, according to the coupled mode theory, their field evolution along the z-direction need to be described as [29]

$$\frac{\partial a(z)}{\partial z} = -j\beta_a a(z) + j\kappa_{ab} b(z) \tag{2.14.a}$$

$$\frac{\partial b(z)}{\partial z} = j\kappa_{ba} a(z) - j\beta_b b(z) \tag{2.14.b}$$

where κ_{ab} and κ_{ba} are defined as the coupling coefficients, which characterize the coupling effect between the two modes. Notice that due to the existence of the coupling effect, the equivalent propagation constant β for the two single waveguide modes are no longer β_a and β_b, but what need to be solved from (2.14).

The coupled mode equations can be written in the form of a matrix equation as:

$$\frac{\partial}{\partial z}\begin{pmatrix} a(z) \\ b(z) \end{pmatrix} = -j\begin{pmatrix} \beta_a & -\kappa_{ab} \\ -\kappa_{ba} & \beta_b \end{pmatrix}\begin{pmatrix} a(z) \\ b(z) \end{pmatrix} = -\underline{\underline{M}}\begin{pmatrix} a(z) \\ b(z) \end{pmatrix} \tag{2.15}$$

and the eigen solution $\begin{pmatrix} a(z) \\ b(z) \end{pmatrix}$ can have a form of

$$\begin{pmatrix} a(z) \\ b(z) \end{pmatrix} = \begin{pmatrix} A \\ B \end{pmatrix} e^{-j\beta z} \tag{2.16}$$

where β is the variable in (2.14) and represents the equivalent propagation constant of the a mode, and A, B are amplitude coefficients of mode a and mode b respectively. Inserting (2.16) into (2.15) can provide the eigenvalue equation as:

$$(\underline{\underline{M}} - \beta \underline{\underline{I}})\begin{pmatrix} A \\ B \end{pmatrix} = 0 \tag{2.17}$$

where $\underline{\underline{I}}$ is the identity matrix. Solving (2.17) gives us the expression of the eigenvalue β as [29]

$$\beta = \frac{\beta_a + \beta_b}{2} \pm \sqrt{\left(\frac{\beta_a - \beta_b}{2}\right)^2 + \kappa_{ab}\kappa_{ba}}. \tag{2.18}$$

Consider in a narrow range of frequencies, β_a and β_b are approximately linear functions of the frequency, which can be observed in Fig. 2.3. Then for the two propagating modes, if their dispersion curves for the isolated single waveguides intersect at $\omega = \omega_c$, so that $\beta_a(\omega_c) = \beta_b(\omega_c) = \beta_c$, these two modes will couple with each other in the geometry of parallel slab waveguides. However, the actual propagation constants of the two coupled modes will be: $\beta = \beta_c \pm \sqrt{\kappa_{ab}\kappa_{ba}}$. In general, the coupling coefficients κ_{ab} and κ_{ba} are complex number. However, in lossless system, it can be derived that $\kappa_{ab} = \kappa_{ba}^*$ for the two coupled modes with same propagating direction. In this scenario, we can get that $\beta = \beta_c \pm \sqrt{\kappa_{ab}\kappa_{ba}} = \beta_c \pm \sqrt{|\kappa_{ab}|^2}$, where the difference of the two eigenvalues β is resulted from and influenced by the coupling coefficients κ_{ab} (or κ_{ba}). Meanwhile, it should be noted that the coupling effect happens not only at $\omega = \omega_c$, but in a narrow range of frequencies centered at ω_c. This result explains the veering phenomenon in Fig. 2.6, which clearly indicates that the two modes in the veering region are coupled to each other.

Chapter 3

Multilayer Waveguide Structure with Periodic Grating — Floquet-Bloch Analysis

3.1 Introduction

An optical waveguiding structure with a periodic grating is a basic configuration for several integrated photonic devices, such as distributed feedback laser cavities, distributed Bragg reflectors, grating-assisted directional couplers, etc. As plane waves are natural modes for uniform multilayer systems, Floquet-Bloch waves are natural modes for periodic multilayer waveguiding structures [30]. In this chapter, we carry out the Floquet-Bloch analysis to solve the dispersion relation, which provides critical insight into the mode behavior inside the structure. The fundamental TE mode is analyzed here. The simple geometry of interest is a single slab waveguide with a periodic grating on its top, all surrounded by cladding media. The method can be easily implemented to solve for both TE and TM modes, as well as for arbitrary multilayer systems with a periodic grating structure. The dispersion phenomenon is analyzed in detail, along with the mode profile illustrated.

3.2 Floquet-Bloch Analysis

This section deals with the method of Floquet-Bloch analysis, which is based on the analysis presented in [22]. The geometry of the system is similar to that which we analyzed in chapter 2, while the difference is the addition of a periodic grating layer (See Fig. 3.1). The

new parameters that characterize the structure are the grating period Λ and the grating height t. Notice that layer k is the grating layer and $x = x_{k-1}$, $x = x_k$ are its boundaries.

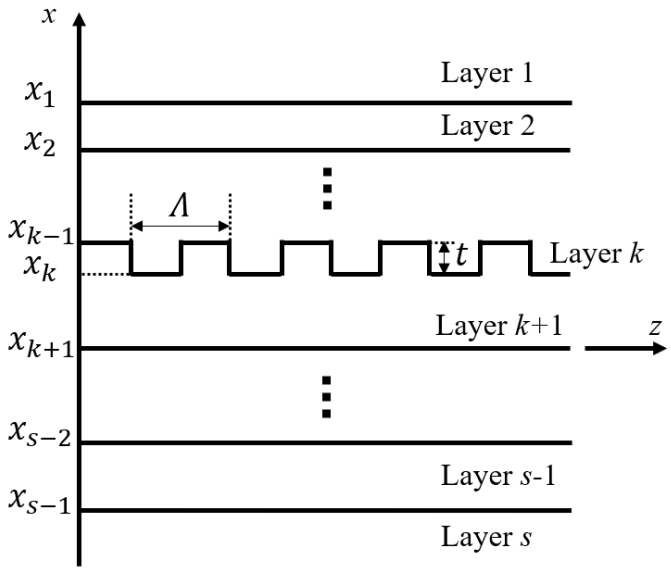

Fig. 3. 1. Basic schematic of a multilayer system with a grating structure. Layers are ordered along the *x*-axis, layer 1 and s are superstrate and substrate respectively, which are assumed to be semi-infinite regions. Layer *k* is the grating layer. $x=x_i$ is the interface between the i^{th} and the $(i+1)^{th}$ layer. Each layer consists of one type of isotropic and homogeneous material, and ε_i is the relative dielectric constant of the i^{th} layer. The structure is assumed to be infinite along the *y*-direction.

According to the Floquet-Bloch theorem, when a wave propagates in an infinite unbounded periodic media, its field along the propagating direction is periodic and can be expressed in the form of a Fourier series, of which each component is known as a spatial harmonic, or a Floquet-Bloch wave. Consider TE modes in our system, the electric field in each layer can be expressed as

$$E_y^{(i)}(x,z) = \sum_{n=-\infty}^{\infty} E_{yn}^{(i)}(x) \exp(-jk_{zn}z) \tag{3.1}$$

where n denotes the order of the spatial harmonic, and k_{zn} is defined as complex propagation constant for the nth harmonic, which is given by

$$k_{zn} = (\beta + nK) + j\alpha \tag{3.2}$$

where β and α are phase and attenuation constants for the fundamental harmonic $k_{z0} = \beta + j\alpha$. Meanwhile, $K = \frac{2\pi}{\Lambda}$ is defined as the grating vector, so that k_{zn} can also be expressed as: $k_{zn} = k_{z0} + nK$.

To find the physical TE modes in our system, we start with analyzing the uniform (non-periodic) regions, which excludes the grating layer (layer k) and its top and bottom boundaries ($x = x_{k-1}$, $x = x_k$). For field solution of each spatial harmonic $E_{yn}(x)\exp(-jk_{zn}z)$, we use the transfer matrix method introduced in chapter 2. Specifically, for the nth spatial harmonic in the ith layer ($i \neq k$), we can similarly define the amplitude coefficients vectors $\underline{C_n}^{(i)} = \begin{pmatrix} a_n^{(i)} \\ b_n^{(i)} \end{pmatrix}$, as well as the transfer matrices along the x-direction: $\underline{\underline{T_n}}^{(i)}$ and $\underline{\underline{M_n}}^{(i+1)}$ (see chapter 2 and [22]). Following the same procedure in chapter 2 for the nth spatial harmonic, we can relate the amplitude coefficients vectors in layer (k-1) and layer (k+1) with the amplitude coefficients vectors in the super- and substrate, respectively. The relations are

$$\underline{C_n}^{(k-1)} = \underline{\underline{S_n}}\,\underline{C_n}^{(1)} = \begin{pmatrix} s_{n12} b_n^{(1)} \\ s_{n22} b_n^{(1)} \end{pmatrix} \tag{3.3a}$$

$$\underline{C_n}^{(k+1)} = \underline{\underline{R_n}}\,\underline{C_n}^{(s)} = \begin{pmatrix} r_{n11} a_n^{(s)} \\ r_{n21} a_n^{(s)} \end{pmatrix}. \tag{3.3b}$$

Notice that there is a tiny difference between the calculation of $\underline{\underline{S_n}}$, $\underline{\underline{R_n}}$ here and that in chapter 2. Here, $\underline{\underline{S_n}} = \underline{\underline{S_n}}^{(k-2)} \cdots \underline{\underline{S_n}}^{(1)}$ with $\underline{\underline{S_n}}^{(i)} = \left(\underline{\underline{M_n}}^{(i+1)}\right)^{-1} \underline{\underline{T_n}}^{(i)}$, and $\underline{\underline{R_n}} = \underline{\underline{R_n}}^{(k+2)} \cdots \underline{\underline{R_n}}^{(s)}$ with $\underline{\underline{R_n}}^{(i)} = \left(\underline{\underline{T_n}}^{(i-1)}\right)^{-1} \underline{\underline{M_n}}^{(i)}$ (see Ref. 1). $s_{n,ij}$ and $r_{n,ij}$ are the matrix elements of $\underline{\underline{S_n}}$ and $\underline{\underline{R_n}}$, respectively.

Next, we analyze the two boundaries of the grating region, which are $x = x_{k-1}$ and $x = x_k$. We apply the boundary conditions for each harmonic of the TE modes. Specifically, the continuity of $E_{yn}(x)$ and $\frac{\partial E_{yn}(x)}{\partial x}$ are still valid at these two interfaces. After some calculation (see Appendix B), the boundary conditions at the boundaries $x = x_{k-1}$ and $x = x_k$ can be determined as

$$\frac{\partial}{\partial x}\left(E_{yn}^{(k)}(x_{k-1})\right) = v_n E_{yn}^{(k)}(x_{k-1}) \tag{3.4a}$$

$$\frac{\partial}{\partial x}\left(E_{yn}^{(k)}(x_k)\right) = w_n E_{yn}^{(k)}(x_k) \tag{3.4b}$$

respectively, where v_n and w_n are given by

$$v_n = \frac{(s_{n12}t_{n21}^{(k-1)} + s_{n22}t_{n11}^{(k-1)})}{(s_{n12}t_{n11}^{(k-1)} + s_{n22}t_{n12}^{(k-1)})} \tag{3.5a}$$

$$w_n = \frac{(r_{n11}m_{n21}^{(k+1)} + r_{n21}m_{n11}^{(k+1)})}{(r_{n11}m_{n11}^{(k+1)} + r_{n21}m_{n12}^{(k+1)})} \tag{3.5b}$$

where $t_{n,ij}^{k-1}$, $m_{n,ij}^{k+1}$ are the matrix elements of $\underline{\underline{T_n}}^{(k-1)}$ and $\underline{\underline{M_n}}^{(k+1)}$ respectively.

In the following, we will obtain the field solution inside the grating layer. Due to the periodicity of material, the relative dielectric constant in the grating layer should be represented by a Fourier series

$$\varepsilon(x,z) = \sum_{n=-\infty}^{\infty} \varepsilon_n(x)\exp(jnKz). \tag{3.6}$$

Here, for simplicity, we just use $\varepsilon(x,z)$ to represent the relative permittivity in layer k (see [22]). Then, instead of using the scalar wave equations, we need to use the equivalent Maxwell equations (see Appendix A) to describe the TE fields in the grating region

$$-j\omega\mu H_z^{(k)} = \frac{\partial E_y^{(k)}}{\partial x} \tag{3.7a}$$

$$-j\omega\varepsilon E_y^{(k)} - j\frac{1}{\omega\mu}\frac{\partial^2 E_y^{(k)}}{\partial z^2} = \frac{\partial H_z^{(k)}}{\partial x} \tag{3.7b}$$

where $E_y^{(k)}$ is given by (3.1) with $i = k$. $H_z^{(k)}$ is also periodic along the z-direction according to the Floquet-Bloch theorem, and can be written as

$$H_z^{(k)}(x,z) = \sum_{n=-\infty}^{\infty} H_{zn}^{(k)}(x) \exp(-jk_{zn}z). \tag{3.8}$$

By substituting the expressions of $\varepsilon(x,z)$, $E_y^{(k)}$ and $H_z^{(k)}$ into (3.7), we will have two sets of equations with infinite numbers, which are impossible to be completely solved. To address this problem, we select finite number of spatial harmonics to represent the fields. In other words, we truncate the infinite Fourier series to finite ones. Meanwhile, it should be noted that the range and the number of the selected spatial harmonics will critically influence the correctness and accuracy of the results, which needs to be adjusted for different scenarios. In Appendix B, the related derivations are shown in detail. Here, we provide results for when we define the field vectors in the grating layer as

$$\underline{E_y}^{(k)}(x) = \left(E_{y,-j_1}^{(k)}(x), \cdots, E_{y,0}^{(k)}(x), \cdots, E_{y,j_2}^{(k)}(x)\right)^T \tag{3.9a}$$

$$\underline{H_z}^{(k)}(x) = \left(H_{z,-j_1}^{(k)}(x), \cdots, H_{z,0}^{(k)}(x), \cdots, H_{z,j_2}^{(k)}(x)\right)^T \tag{3.9b}$$

and let $l = j_1 + j_2 + 1$ be the number of spatial harmonics we select, then we can transform the equivalent Maxwell equations (3.7) to

$$\frac{\partial}{\partial x}\left(\underline{E_y}^{(k)}(x)\right) = \underline{\underline{Q}}\,\underline{H_z}^{(k)}(x) \tag{3.10a}$$

$$\frac{\partial}{\partial x}\left(\underline{H_z}^{(k)}(x)\right) = \underline{\underline{P}}\,\underline{E_y}^{(k)}(x) \tag{3.10b}$$

where $\underline{\underline{Q}}$ and $\underline{\underline{P}}$ are $l \times l$ square matrices, whose elements are given as

$$q_{mn} = -j\omega\mu\delta_{mn} \tag{3.11a}$$

$$p_{mn} = j\omega\varepsilon_0\left(\left({}^{k_{zn}}/_{k_0}\right)^2 \delta_{nm} - \varepsilon_{n-m}\right). \tag{3.11b}$$

Besides the equivalent Maxwell equations, the boundary conditions at interfaces: $x = x_{k-1}$ and $x = x_k$ can also be expressed in the form of matrix equations, since finite number of spatial harmonics are used to represent the total fields. Specifically, the two boundary conditions are

$$\underline{\underline{U}} \frac{\partial}{\partial x}\left(\underline{E_y}^{(k)}(x_{k-1})\right) = \underline{\underline{V}}\,\underline{E_y}^{(k)}(x_{k-1}) \tag{3.12a}$$

$$\underline{\underline{U}} \frac{\partial}{\partial x}\left(\underline{E_y}^{(k)}(x_k)\right) = \underline{\underline{W}}\,\underline{E_y}^{(k)}(x_k) \tag{3.12b}$$

where $\underline{\underline{U}}$ is $l \times l$ unit matrix, $\underline{\underline{V}}$ and $\underline{\underline{W}}$ are diagonal matrices with same size, which are given by

$$\underline{\underline{V}} = \mathrm{diag}(v_{-j_1} \cdots v_0 \cdots v_{j_2}) \tag{3.13a}$$

$$\underline{\underline{W}} = \mathrm{diag}(w_{-j_1} \cdots w_0 \cdots w_{j_2}). \tag{3.13b}$$

At this stage, we completely describe the TE fields in our system through the equivalent Maxwell equation (3.10) for the grating layer, and the boundary conditions associated with that layer (3.12). To solve the fields and find the supported modes in the structure, we first solve (3.10) numerically via the classical Runge-Kutta method, which has been illustrated in detail in [22]. The resulting equations relate the field values at $x = x_k$ with that at $x = x_{k-1}$ as

$$\underline{E_y}^{(k)}(x_k) = \underline{\underline{Y_E}}\,\underline{E_y}^{(k)}(x_{k-1}) \tag{3.14a}$$

$$\underline{H_z}^{(k)}(x_k) = \underline{\underline{Y_H}}\,\underline{E_y}^{(k)}(x_{k-1}) \tag{3.14b}$$

where $\underline{\underline{Y_E}}$ and $\underline{\underline{Y_H}}$ are the matrices $\underline{\underline{Y_f}}$ and $\underline{\underline{Y_g}}$ defined in [22], respectively. Finally, by combining (3.14) with the boundary conditions (3.12), we obtain the characteristic equation of our system

$$\left(\underline{\underline{U}}\,\underline{\underline{Q}}\,\underline{\underline{Y_H}} - \underline{\underline{W}}\,\underline{\underline{Y_E}}\right)\underline{E_y}^{(k)}(x_{k-1}) = \underline{\underline{F}}\,\underline{E_y}^{(k)}(x_{k-1}) = 0 \tag{3.15}$$

where $\underline{\underline{F}}$ is the coefficients matrix of the characteristic equation, which will have nontrivial solutions if

$$\det(\underline{\underline{F}}) = 0. \tag{3.16}$$

Solving this last equation will give the propagation constants of the TE modes that are supported by the structure. Sweeping the existing propagation constants for frequencies of interest will provide the dispersion relations. Meanwhile, the mode profile for each selected spatial harmonic can be calculated, so that the total field distribution along the *x*-direction can be finally calculated and illustrated. This is done by calculating the field coefficients $\underline{E_y}^{(k)}(x_{k-1})$ by solving (3.15) once the $\underline{\underline{F}}$ matrix is determined from (3.16).

3.3 Single Slab Waveguide with Periodic Grating

In this section, we carry out the Floquet-Bloch theory to analyze a single slab waveguide with a periodic grating structure on its top. The geometry of the structure is shown in Fig. 3.2, where silicon is the material of the waveguiding layer, while the cladding layers are made from silicon dioxide. The grating structure is formed by periodically alternating Si and SiO_2. The waveguiding layer has a thickness of t, while the grating layer is characterized by the grating height h and the grating period Λ.

Using the expounded mathematical model in section 3.2, we solve for the propagating modes with TE polarization in a specific geometry, which has $t = 80$nm, $h = 20$nm, and $\Lambda = 381$nm. To ensure a sufficient accuracy of the calculation, we select 7 spatial harmonics to

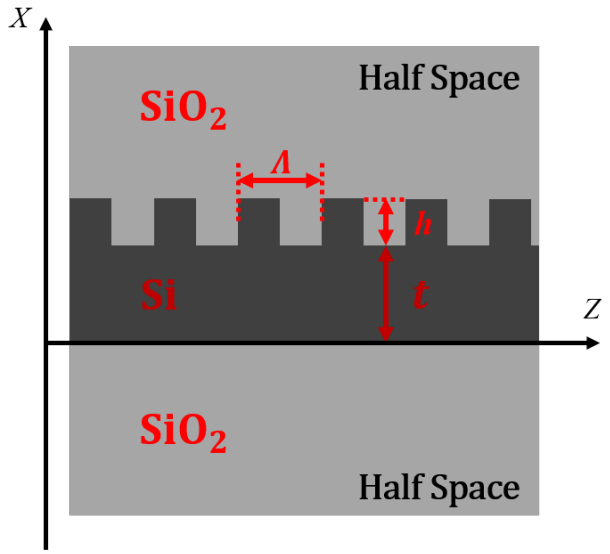

Fig. 3. 2. Geometry of a single slab optical waveguide with a periodic grating on top. The materials for waveguide layer and cladding layers are silicon and silicon dioxide respectively, whose refractive indices are n_{Si}=3.48 and n_{SiO2}=1.444 respectively. The waveguide layer has a thickness of t, the grating layer has a height of h and period of Λ. both the cladding layers are assumed to be semi-infinite layers.

represent the total field (i.e. from the -3rd to the 3rd harmonic) [22], [31]. The dispersion diagrams are shown in Fig. 3.3. In general, the single slab waveguide with periodic grating is a type of one-dimensional photonic crystals, whose dispersion characteristics have been well studied [32]–[35]. In the following, we represent its dispersion diagrams and analyze the mode behaviors in terms of the mode degeneracy.

In Fig. 3.3, the frequencies of interest are normalized by the center angular frequency ω_0, which corresponds to the optical free-space wavelength 1550nm. The propagation constants are calculated for fundamental spatial harmonic and normalized by $\frac{\pi}{\Lambda}$, which equals a half of the grating vector K. Recall that the propagation constants for the propagating modes are pure real numbers in a lossless system, i.e. the α in (3.2) is zero. In Fig. 3.3(a), the SiO_2 light line separates the leaky modes from the propagating bounded modes. The dispersion characteristics of propagating modes are displayed for a wide range

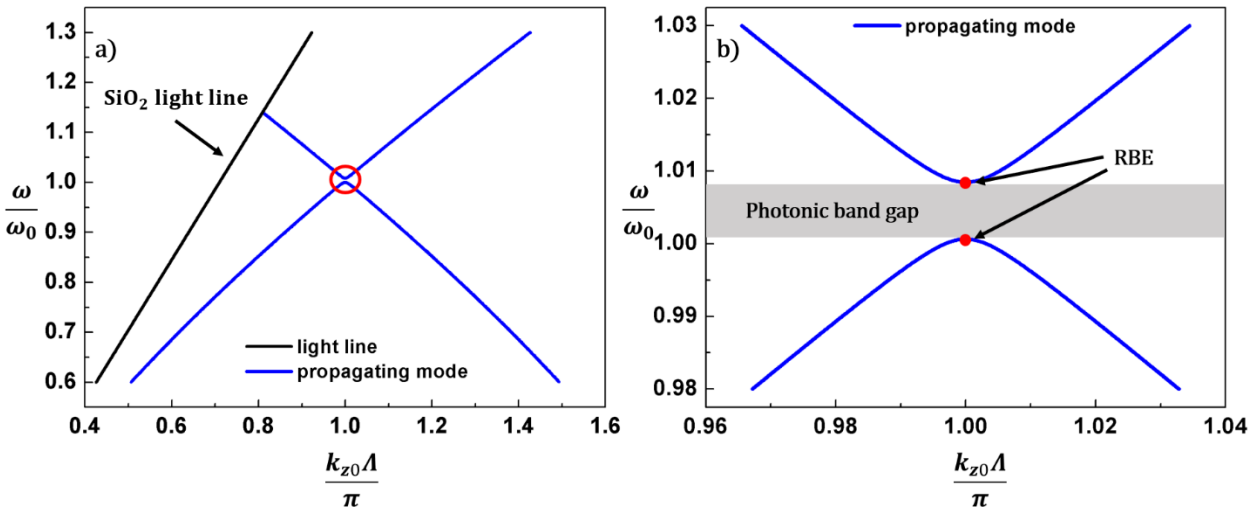

Fig. 3. 3. Dispersion diagrams of propagating modes. a) dispersion diagram for a wide range of frequency, the SiO_2 light line defines the region of propagating modes, b) dispersion diagram near the band gap, where the band gap is labelled by a gray strip with the regular band edges marked by red dots.

of frequencies, where the most important feature is marked by a red ring, zoomed in, and displayed in Fig. 3.3(b). From Fig. 3.3(b), one can find that in a range of frequencies (the bandgap), there are no propagating modes supported in the system. This gap between the upper and lower dispersion curves is known as a photonic band gap in terms of the band structure of the photonic crystals [32]. The two vertices of the two dispersion curves are known as the photonic band edges, where the propagating modes coalesce, and become degenerate modes [4]. Specifically, taking the lower dispersion curve as an example, one can find that with increasing the frequency, the propagation constants of the two modes (one at the left branch, the other at the right branch) get closer until they are both equal to $\frac{\pi}{\Lambda}$ at the band edge and merge to form a degenerate mode. (The structure is designed to have a band edge in very close proximity to ω_0.) In this case, the photonic band edge is known as the regular band edge because two modes are involved in the mode degeneracy.

Using the expounded mathematical model in section 3.2, we solve for the propagating

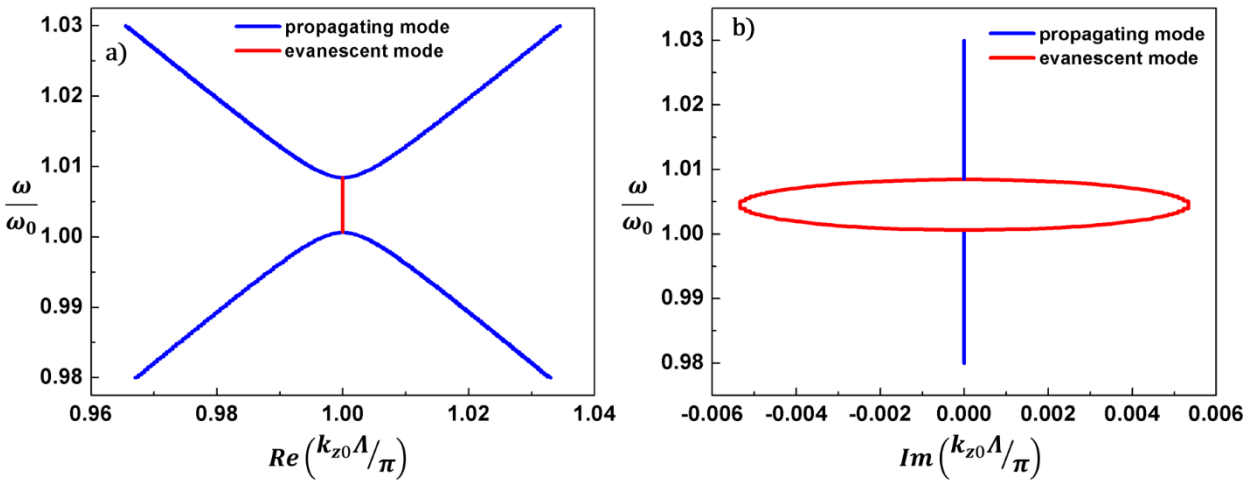

Fig. 3. 4. Dispersion diagrams for both propagating and evanescent modes near the band gap. a) dispersion diagram for the real parts of the propagation constants, b) dispersion diagram for the imaginary parts of the propagation constant.

modes with TE polarization in a specific geometry, which has $t = 80\text{nm}$, $h = 20\text{nm}$, and $\Lambda = 381\text{nm}$. To ensure a sufficient accuracy of the calculation, we select 7 spatial harmonics to can be found that both propagating modes and evanescent modes in our system exist at those frequencies. The corresponding dispersion diagrams are shown in Fig. 3.4, where Fig. 3.4(a) and (b) display the dispersion relations with respect to the real and the imaginary parts of the propagation constants, respectively. It is clear that the modes inside the bandgap are evanescent modes, whose propagation constants have equal real parts and imaginary parts of opposite signs. The difference between the two imaginary values is maximum at the center of the band gap.

To gain a better inspection of the modes at the band edge, the total field distribution is calculated and plotted, along with the mode profiles of the fundamental and the -1st harmonics, at the frequency corresponding to the lower band edge. We consider the modal solution associated to the modal propagation from (3.1), namely $E_y^{(i)}(x,z) = \sum_{n=-\infty}^{\infty} E_{yn}^{(i)}(x)\exp(-jk_{zn}z)$, with $k_{z0} = \pi/\Lambda$. The total field is the summation of the fields of

the selected harmonic (7 in this case). The calculating method is that: first, through plugging the calculated fundamental propagation constant k_{z0} into (3.15), we can obtain the field value of each harmonic at the upper boundary of the grating layer. Specifically, to solve equation (3.15), the field value of the fundamental harmonic at x_{k-1} is assumed as unitary, (i.e., we assume $E_{y0}^{(k)}(x_{k-1}) = 1$). Then, the field distribution inside the grating layer can be calculated through the Runge-Kutta method [22], while the field distribution outside the grating layer can be finally obtained through the transfer matrix method (3.3).

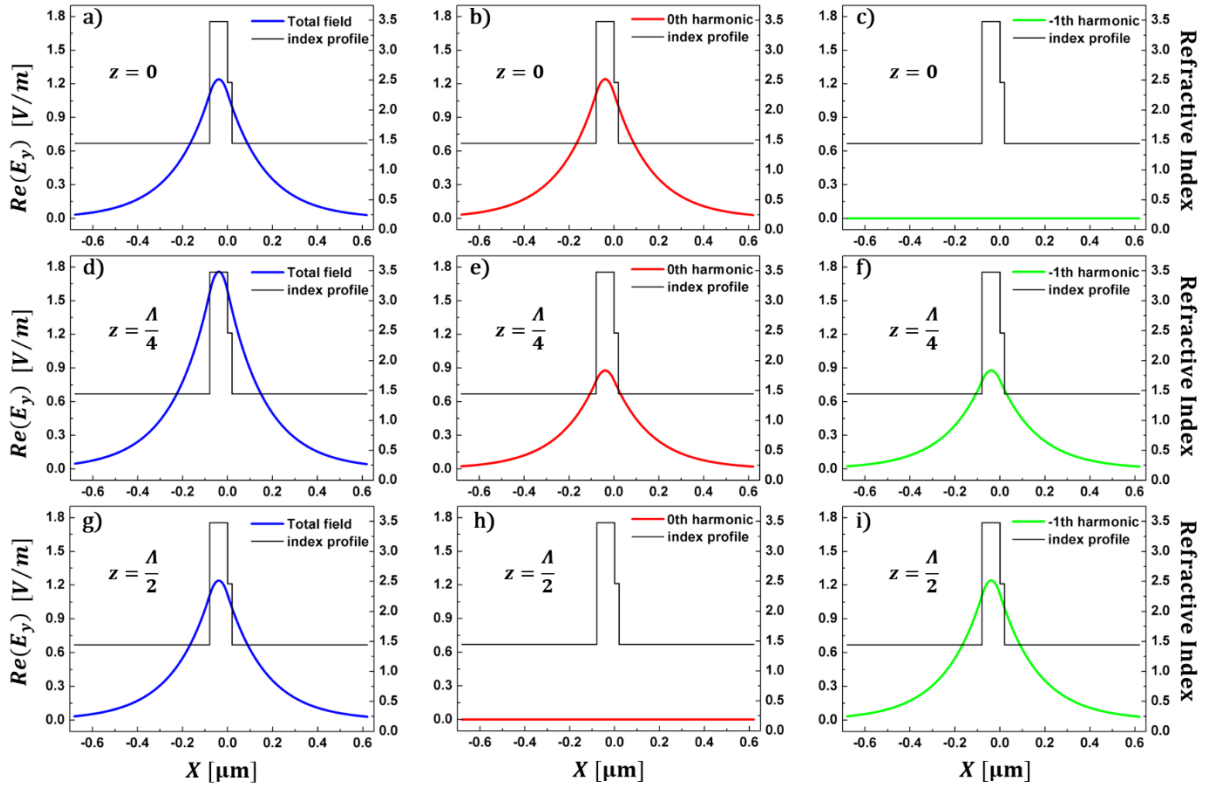

Fig. 3. 5. Field distributions and refractive indices' profiles at z=0 (figure (a)-(c)), z=$\Lambda/4$ (figure (d)-(f)), and z=$\Lambda/2$ (figure (g)-(i)). The field distributions are plotted for the total field (figure (a)(d)(g)), the fundamental harmonic (figure (b)((e)(h)), and the -1st harmonic (figure (c)(f)(i)). The refractive index of the grating layer is calculated through averaging the refractive indices of Si and SiO_2.

In general, the calculated electric fields at the lower band edge have complex values, whose real parts represent the field magnitude and the imaginary parts represent the phases.

In Fig. 3.5, the real parts of the electric fields are extracted and plotted. Meanwhile, the refractive indices' profiles are also plotted to illustrate the geometry. The refractive index of the grating layer is here (in the plot, solid black line) calculated by $\frac{n_{\mathrm{Si}}+n_{\mathrm{SiO2}}}{2}$, which represents an average refractive index of the grating region.

Figs. 3.5(a)-(c) show the results calculated through solving the characteristic equation as well as conducting the Runge-Kutta method and the transfer matrix method as explained before. Fig. 3.5(a) shows the total field distribution along the *x*-direction, where one can find that light is confined in the waveguide and grating regions, with a TE0-like field profile. Fig. 3.5(b), (c) plot the *x*-distribution of the fundamental and the -1st harmonic respectively. Then, it is worth noting that the field distributions along the *x*-direction are not static, but they are evolving along the *z*-direction. The results shown in Figs. 3.5(a)-(c) can be considered as the fields at $z = 0$, (i.e. $E_{yn}^{(i)}(x, 0)$) because $e^{-jk_{zn}\cdot 0} = 1$ is true for each harmonic in (3.1). For each harmonic, how the *x*-dependent field evolution varies along z is calculated as $E_{yn}^{(i)}(x, z) = E_{yn}^{(i)}(x, 0)\exp(-jk_{zn}z)$, where k_{zn} is determined by (3.2) with the calculated k_{z0}. The total field distribution along the *x*-direction at a certain *z*-location can be calculated by summing field values of all the 7 harmonics. Fig. 3.5(a), (d) and (g) shows the total field distribution along the *x*-direction at three different z location. The *z*-evolutions of the fundamental and the -1st harmonic are plotted in Fig. 3.5(b)(e)(h) and (c)(f)(i) respectively. Comparing the results in Fig. 3.5, one can find that the fundamental and the -1st spatial harmonics are dominant Floquet modes in the structure. They dominate the total field alternatively as the wave evolve along the *z*-direction, while field values (distributions) of other harmonics are negligible.

Chapter 4

Multilayer Waveguide Structure with Periodic Grating — Coupled Mode Theory

4.1 Introduction

In this chapter, the coupled mode theory is implemented to provide a better understanding for the wave coupling of the modes in multilayer waveguide structure with grating. Coupled mode theory has been widely adopted to analyze the waveguiding structures with periodic gratings [2], [29], [36], [37]. Single slab waveguide with periodic grating is first analyzed to illustrate a basic coupled-mode model to characterize the coupling effects in periodic waveguide structure. Then a parallel slab waveguide structure with grating is proposed, and a modified coupled-mode model is developed correspondingly [38]. The degeneracy conditions of four modes is discussed in the parallel slab waveguide structure with grating. The existence of degenerate band edge in that scenario is finally stated and qualitatively illustrated.

4.2 Single Slab Waveguide with Periodic Grating

In this section, we implement the well-known coupled mode theory to analyze the modes coupling effects provided by a periodic grating structure, and the method we applied here is based on [29]. The geometry of interest is same as what is treated in Ch. 3, namely, a single slab waveguide with a periodic grating structure on top. According to the coupled

mode theory, the periodic grating is treated as a spatial perturbation added on the waveguiding layer of the uniform multilayer system [29]. The dielectric constants' distribution $\varepsilon(x,z)$ of the whole system can be divided into two parts, of which the first part $\varepsilon^{(0)}(x)$ is defined as the dielectric constants' distribution of the uniform layered system, while the second part $\Delta\varepsilon(x,z)$ describe the periodic perturbation on the dielectric constants. Then, we can have $\varepsilon(x,z) = \varepsilon^{(0)}(x) + \Delta\varepsilon(x,z)$. Due to the periodicity of $\Delta\varepsilon(x,z)$, it can be described as

$$\Delta\varepsilon(x,z) = \varepsilon_0 \sum_{p\neq 0} \Delta\varepsilon_p(x) e^{jp\frac{2\pi}{\Lambda}z} \tag{4.1}$$

where ε_0 is the dielectric constant in free space and $\Delta\varepsilon_p(x)$ is the pth order Fourier harmonics. In lossless systems, the relative dielectric constants are real numbers so that $\Delta\varepsilon_p^* = \Delta\varepsilon_{-p}$.

First, consider a uniform single slab waveguide system without the periodic perturbation. Assume that the waveguide layer only supports the fundamental TE mode, whose electric field can be expressed as a scalar function: $E_y = E_y(x)e^{-j\beta_0 z}$, where β_0 is the phase constant for the field propagation. In the uniform systems, the electric field of the TE modes satisfy the wave equation [29]

$$\left[\frac{\partial^2}{\partial x^2} + \frac{\partial^2}{\partial z^2} + \omega^2\mu\varepsilon^{(0)}(x)\right] \cdot E_y(x)e^{\pm j\beta_0 z} = 0 \tag{4.2}$$

where $E_y(x)e^{\pm j\beta_0 z}$ describes the modes that propagates in opposite directions. Then, if taking the spatial perturbation into account, the composed dielectric constants $\varepsilon(x,z)$ need to be implemented and the TE modes' wave equation is modified as [29]

$$\left[\frac{\partial^2}{\partial x^2} + \frac{\partial^2}{\partial z^2} + \omega^2\mu\varepsilon^{(0)}(x)\right] E_y = -\omega^2\mu\Delta\varepsilon(x,z)E_y. \tag{4.3}$$

To implement the coupled mode theory, we assume there are two TE-polarized waves propagates in opposite direction in the system and define the amplitude coefficients function $A_+(z)$ and $A_-(z)$ for each wave, which describe the evolution of the field amplitudes along the propagating direction. Then, the total field in the structure equals the superposition of the two oppositely propagating fields

$$\left[A_+(z)e^{-j\beta_0 z} + A_-(z)e^{j\beta_0 z}\right]E_y(x). \tag{4.4}$$

Inserting (3.20) into (3.19) and conduct some derivations [29], one can find that when $\beta_0 \approx pK - \beta_0$ with $K = \frac{2\pi}{\Lambda}$ being the grating vector, the two oppositely propagating modes are strongly coupled. In our scenario, $p = 1$. Then, we can further define $\beta_B = \frac{p\cdot K}{2} = \frac{\pi}{\Lambda}$ and $\Delta\beta = \beta_0 - \beta_B$ as well as make the transform $a_+(z) = A_+(z)e^{-j\Delta\beta z}$, $a_-(z) = A_-(z)e^{j\Delta\beta z}$. After some derivation, the coupled mode equation that describe the coupling effects between the two oppositely propagating modes in our system can be obtained as [29]

$$\frac{\partial}{\partial z}\begin{pmatrix} a_+(z) \\ a_-(z) \end{pmatrix} = -j\begin{pmatrix} \Delta\beta & \chi_{a_\pm} \\ \chi_{a_\mp} & -\Delta\beta \end{pmatrix}\begin{pmatrix} a_+(z) \\ a_-(z) \end{pmatrix} \tag{4.5}$$

which has similar form of the coupled mode equation discussed in chapter 2. Here, $\chi_{a_\pm}$ and $\chi_{a_\mp}$ are defined as the coupling coefficients of the two oppositely propagating modes, whose expressions are given in [29]. Like the procedure we followed in chapter 2, the equivalent propagation constant of the two oppositely propagating modes β can be solved in the scenario of eigenvalue problem [29], and its expression is given as

$$\beta = \beta_B \pm \sqrt{\Delta\beta^2 + \chi_{a_\pm}\chi_{a_\mp}} \tag{4.6}$$

where $\chi_{a_\pm}$ and $\chi_{a_\mp}$ are complex numbers in general. However, in lossless systems, $\chi_{a_\mp} = -\chi^*_{a\pm}$, and $\chi_{a_\mp} \cdot \chi_{a_\pm} = -\left|\chi_{a_\pm}\right|^2$, therefore we have:

$$\beta = \beta_B \pm \sqrt{\Delta\beta^2 - \left|\chi_{a_\pm}\right|^2}\,. \tag{4.7}$$

From this equation, one can find that when $|\Delta\beta| < \left|\chi_{a_\pm}\right|$, the equivalent propagation constant β is a complex number, in other words propagating modes are not supported but there will exist evanescent modes. Since the propagation constants are functions of frequency, the photonic band gap can be interpreted as the range of frequencies where the corresponding propagation constants satisfy the $|\Delta\beta| < \left|\chi_{a_\pm}\right|$.

4.3 Degenerate Band Edge

In this section we discuss the degeneracy conditions of four modes in multilayer waveguide structures with grating. In the previous chapter, we have illustrated that a single slab waveguide with a grating on top exhibits second order degeneracy, namely, it is a regular band edge due to coalescing of two identical modes propagating opposite to each other. Therefore, to obtain a fourth order degeneracy or a degenerate photonic band edge, i.e., coalescing of four modes, we need to at least two coupled slab waveguides with grating, as shown in Fig. 4.1., to be able to support four modes, which are for instance even and odd mode propagating in positive and negative z-direction for symmetrical structure. This type of structure has been proposed and analyzed in terms of the grating-assisted directional couplers (GADC) [38]–[41]. However, these GADC systems operate either near or far away the photonic band edge [39], so that only two modes are coupled which is assisted by the grating structure. In the following section, we implement a coupled-mode model that is reported in detail in [38], and analyze the situation that four supported modes mutually

couple to each other. Finally, the four-mode degeneracy condition is qualitatively discussed and illustrated based on this coupled-mode model.

In the following, the system of coupled slab waveguides with periodic grating is analyzed, whose geometry is shown in Fig. 4.1. The geometry can be regarded as a combination of the coupled slab waveguides shown in Fig. 2.5 and the single periodic waveguide structure shown in Fig. 3.2, however, for the top layer we use silicon instead of indium phosphide. For the convenience of the following derivation, the upper and lower waveguides are denoted as waveguide A and B respectively, and each waveguide is assumed to support only a fundamental TE mode.

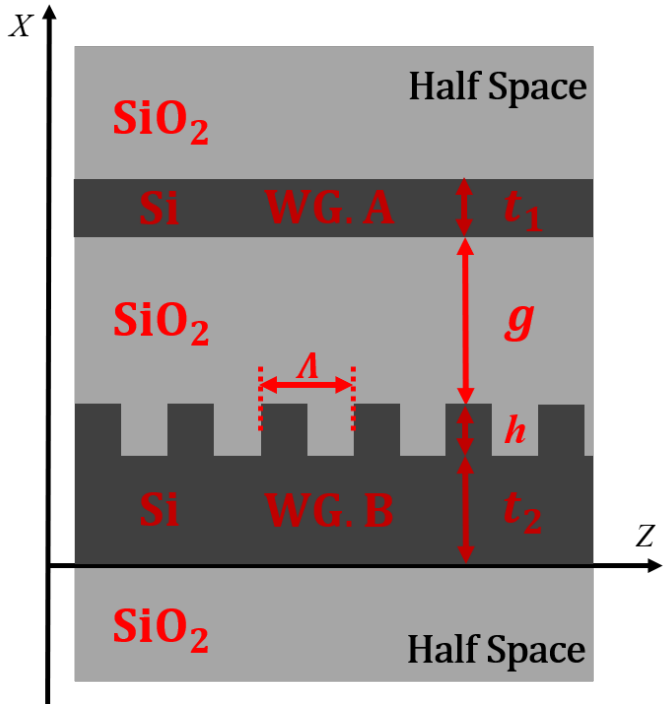

Fig. 4. 1. Proposed structure that exhibits a degenerate photonic band edge: there is coupling between a regular dielectric slab waveguide and another one with grating. The materials for waveguide layer and cladding layers are silicon and silicon dioxide respectively, whose refractive indices are $n_{\mathrm{Si}} = 3.48$ and $n_{\mathrm{SiO_2}} = 1.444$ respectively.

The model we adopt here is based a coupled-mode model for four mutually-coupled modes introduced in [38]. It is worth noting that a refined model has been developed and

introduced in [40]–[43], however, for qualitative discussion, the model in [38] is sufficient and straightforward to describe the complete coupling mechanism in the structure shown in Fig. 4.1. Meanwhile, it is also worth noting that the technique to develop the coupled mode model in [38] is same as that introduced in Ch. 2 and the previous section. The total electric field in the structure can be written in the form

$$E_y(x,z) = \left[A_+(z)e^{-j\beta_a z} + A_-(z)e^{j\beta_a z}\right]E_y^{(a)}(x) + \left[B_+(z)e^{-j\beta_b z} + B_-(z)e^{j\beta_b z}\right]E_y^{(b)}(x) \tag{4.8}$$

where $E_y^{(a)}(x)$ and $E_y^{(b)}(x)$ are field distributions of the single waveguide modes in waveguide A and B, respectively, β_a and β_b are phase constants of the single waveguide modes in waveguide A and B respectively, and $A_\pm(z)$, $B_\pm(z)$ are defined as the amplitude coefficients functions along the z-direction for the opposite propagating modes in waveguide A and B, respectively. In equation (4.7), four individual modes are given, and the total field is represented as their superposition. Then, similar to the procedure we conducted in the previous section, we can further define $\beta_B = \frac{\pi}{\Lambda}$, $\Delta\beta_a = \beta_a - \beta_B$, as well as $\Delta\beta_b = \beta_b - \beta_B$, and make the transform:

$$a_\pm(z) = A_\pm(z)e^{\mp j\Delta\beta_a z} \tag{4.9a}$$

$$b_\pm(z) = B_\pm(z)e^{\mp j\Delta\beta_b z}\,. \tag{4.9b}$$

Based on (4.8), the coupled mode equation that describes the complete coupling mechanism in the system can be expressed as [38]

$$\frac{d}{dz}\begin{pmatrix} a_+(z) \\ a_-(z) \\ b_+(z) \\ b_-(z) \end{pmatrix} = -j\begin{pmatrix} \Delta\beta_a & \chi_{a_\pm} & -\kappa_{ab} & \chi_{ab} \\ \chi_{a_\mp} & -\Delta\beta_a & \chi_{ba} & \kappa_{ab} \\ -\kappa_{ba} & \chi_{ab} & \Delta\beta_b & \chi_{b_\pm} \\ \chi_{ba} & \kappa_{ba} & \chi_{b_\mp} & -\Delta\beta_b \end{pmatrix}\begin{pmatrix} a_+(z) \\ a_-(z) \\ b_+(z) \\ b_-(z) \end{pmatrix} \tag{4.10}$$

where κ_{ab}, κ_{ba}, $\chi_{a_\pm}$ and $\chi_{b_\pm}$ have same definitions with those in chapter 2 and in the previous section. κ_{ab} and κ_{ba} describe the co-directional coupling effect between the individual modes in waveguide A and B. $\chi_{a_\pm}$ and $\chi_{b_\pm}$ are named as the self-Bragg coupling coefficients that describe the contra-directional coupling effect between the opposite propagating individual modes in waveguide A and B respectively. The new parameters here are χ_{ab} and χ_{ba}, whose expressions can be found in [38]. These two parameters are called exchange-Bragg coupling coefficients, which describe the coupling effects between one individual mode in waveguide A (or B) and the other individual mode that propagates in opposite direction in waveguide B (or A).

Having determined the coupled mode equation, the equivalent propagation constants of the four individual modes in the system can be obtained through solving the eigenvalue problem (see Ch. 2, and [38]). The four equivalent propagation constants of the four individual modes are given by a simplified expression

$$\beta_1 = \beta_B + \sqrt{A + \sqrt{D}} \tag{4.11a}$$

$$\beta_2 = \beta_B - \sqrt{A + \sqrt{D}} \tag{4.11b}$$

$$\beta_3 = \beta_B + \sqrt{A - \sqrt{D}} \tag{4.11c}$$

$$\beta_4 = \beta_B - \sqrt{A - \sqrt{D}} \tag{4.11d}$$

where A and D are functions of all the coefficients matrix elements in (4.10). The expressions of A and D are given in [38].

In analog to the regular band edges, when the four modes are coalescing at the degenerate band edge, they are supposed to have same propagation constants, which should

be equal to β_B according to (4.11), i.e. $\beta_1 = \beta_2 = \beta_3 = \beta_4 = \beta_B$. From (4.11), it is easily to find that the necessary condition to achieve a four-mode degeneracy is $A = D = 0$.

For simplicity we assume that the propagation constants of the single waveguide modes β_a and β_b are linear functions of the free-space wavenumber k_0, which corresponds to the center angular frequency ω_0, with the relations $\beta_a = k_0 n_{eff,a}$ and $\beta_b = k_0 n_{eff,b}$ respectively, where $n_{eff,a}$ and $n_{eff,b}$ are defined as the effective refractive index of the two single waveguide modes respectively, $k_0 = \frac{\omega_0}{c}$, with c is the speed of light in free space. Finally, to achieve the four-mode degeneracy at a center angular frequency ω_0, we first assume certain values of $n_{eff,a}$, $n_{eff,b}$ and β_B, then the values of $\Delta\beta_a$ and $\Delta\beta_b$ can be calculated for the desired center angular frequency. Next, through sweeping the values of the multiple coupling coefficients in some range [38], one may find a combination of coupling coefficients that satisfy the equation: $A = D = 0$, i.e. the necessary condition for the degenerate band edge. To try to find the degenerate band edge, we first assume the

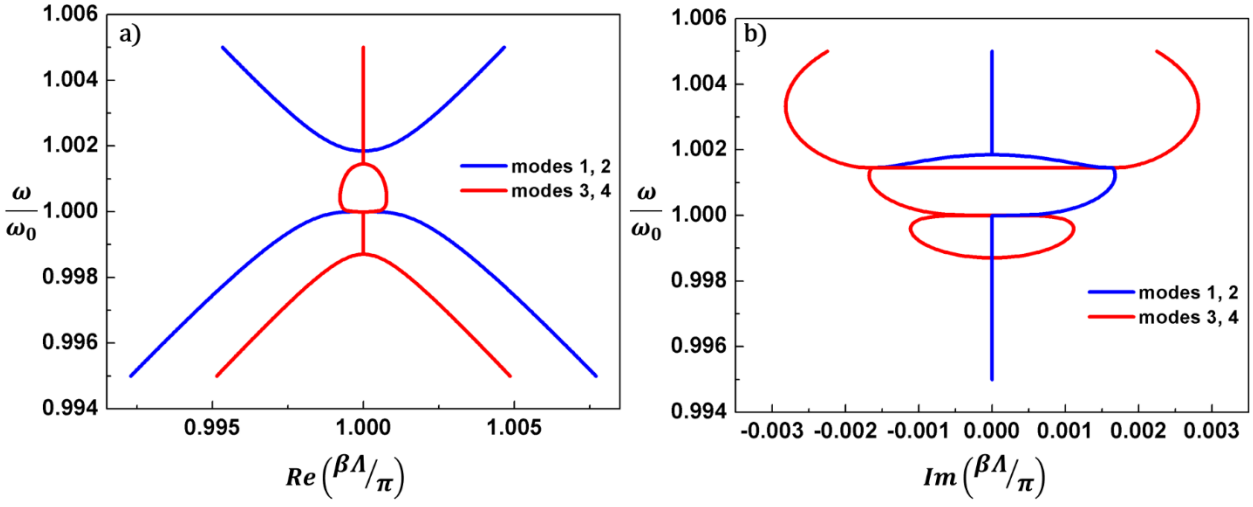

Fig. 4. 2. Dispersion diagrams of a coupled slab waveguide structure with a periodic grating. a) Dispersion diagram for the real parts of the propagation constants, and b) Dispersion diagram for the imaginary part of the propagation constants.

effective refractive indices $n_{eff,a} = 3.19$, $n_{eff,b} = 3.2$, [38] and the $\beta_B = 1.2973 \times 10^7\ {}^{rad}/_{m}$, and find the desired combinations of coupling coefficients. As a result, several combinations of coupling coefficients can be found, which indicates that the degenerate band edges can be achieved in the scenario of coupled slab waveguides with a periodic grating. The dispersion diagrams calculated from one combination of coupling coefficients are shown in Fig. 4.2 to illustrate a possible situation of the DBE, where Fig. 4.2 (a), (b) show the dispersion diagrams for the real and imaginary parts of the equivalent propagation constant respectively. The solid blue curves correspond to β_1 and β_2, the red curves correspond to β_3 and β_4. From Fig. 4.2, one can find that four modes merge to a degenerate mode when $\omega = \omega_0$, which indicates the fourth order mode degeneracy or the degenerate band edge. Meanwhile, the dispersion curves near the degenerate band edge are flat, which exhibits the same features of the analogous situations reported in [4], [8]

Finally, it should be noted that here we only qualitatively illustrate the existence of DBE in our system. To verify its authenticity, exact solution of degenerate mode related to a precise structure need to be further provided following the scheme in Chapter 3.

Chapter 5

Conclusion and Future Work

5.1 Conclusion

Modes behavior has been rigorously analyzed in various multilayer waveguide structures with grating. Dispersion characteristics for both propagating modes and evanescent modes have been obtained. The propagating modes in the multilayer waveguide structures with grating have been thoroughly studied in terms of field distribution along the transverse direction, and field evolution along the propagating direction. Modes coupling effects have been qualitatively analyzed via coupled mode theory, and quantitatively demonstrated through transfer matrix method as well as Floquet-Bloch analysis. The dispersion characteristic resulted from co-directional coupling and contra-directional have been illustrated. Modes degeneracy conditions as well as regular and degenerate photonic band edges were emphatically elaborated.

5.2 Future Work

Based on the work of this report, investigation on modes can be conducted for more complicated geometries as well as for more attracting topics. Rigorous demonstration of the fourth-order mode degeneracy is the immediate target. Through changing the geometries, coupling effects among modes can be delicately adjusted, and it can be expected that the degenerate band edge will be achieved in the following explorations.

Bibliography

[1] J. J. Degnan, "The waveguide laser: A review," *Appl. Phys.*, vol. 11, no. 1, pp. 1–33, Sep. 1976.

[2] H. Kogelnik and C. V. Shank, "Coupled-Wave Theory of Distributed Feedback Lasers," *J. Appl. Phys.*, vol. 43, no. 5, pp. 2327–2335, May 1972.

[3] S. Wang, "Principles of distributed feedback and distributed Bragg-reflector lasers," *IEEE J. Quantum Electron.*, vol. 10, no. 4, pp. 413–427, Apr. 1974.

[4] M. Y. Nada, M. A. Othman, and F. Capolino, "Theory of coupled resonator optical waveguides exhibiting high-order exceptional points of degeneracy," *Phys. Rev. B*, vol. 96, no. 18, p. 184304, 2017.

[5] M. G. Wood, J. R. Burr, and R. M. Reano, "Degenerate band edge resonances in periodic silicon ridge waveguides," *Opt. Lett.*, vol. 40, no. 11, pp. 2493–2496, Jun. 2015.

[6] R. Kazarinov and C. Henry, "Second-order distributed feedback lasers with mode selection provided by first-order radiation losses," *IEEE J. Quantum Electron.*, vol. 21, no. 2, pp. 144–150, Feb. 1985.

[7] M. A. K. Othman, F. Yazdi, A. Figotin, and F. Capolino, "Giant gain enhancement in photonic crystals with a degenerate band edge," *Phys. Rev. B*, vol. 93, no. 2, p. 024301, Jan. 2016.

[8] M. Veysi, M. A. Othman, A. Figotin, and F. Capolino, "Degenerate band edge laser," *Phys. Rev. B*, vol. 97, no. 19, p. 195107, 2018.

[9] N. Gutman, L. C. Botten, A. A. Sukhorukov, and C. M. de Sterke, "Degenerate band edges in optical fiber with multiple grating: efficient coupling to slow light," *Opt. Lett.*, vol. 36, no. 16, pp. 3257–3259, Aug. 2011.

[10] "OSA | Slow light with flat or offset band edges in few-mode fiber with two gratings." [Online]. Available: https://www.osapublishing.org/oe/abstract.cfm?uri=OE-15-26-17954. [Accessed: 06-Jun-2018].

[11] J. R. Burr and R. M. Reano, "Zero-coupling-gap degenerate band edge resonators in silicon photonics," *Opt. Express*, vol. 23, no. 24, pp. 30933–30942, Nov. 2015.

[12] R. Soref, "The Past, Present, and Future of Silicon Photonics," *IEEE J. Sel. Top. Quantum Electron.*, vol. 12, no. 6, pp. 1678–1687, Nov. 2006.

[13] "OSA | Energy-Efficient Photonics in Future High-Connectivity Computing Systems." [Online]. Available: https://www.osapublishing.org/jlt/abstract.cfm?uri=jlt-33-4-889. [Accessed: 06-Jun-2018].

[14] P. Kozma, F. Kehl, E. Ehrentreich-Förster, C. Stamm, and F. F. Bier, "Integrated planar optical waveguide interferometer biosensors: A comparative review," *Biosens. Bioelectron.*, vol. 58, pp. 287–307, Aug. 2014.

[15] M. Yamada and K. Sakuda, "Analysis of almost-periodic distributed feedback slab waveguides via a fundamental matrix approach," *Appl. Opt.*, vol. 26, no. 16, pp. 3474–3478, Aug. 1987.

[16] S. S. Wang and R. Magnusson, "Theory and applications of guided-mode resonance filters," *Appl. Opt.*, vol. 32, no. 14, pp. 2606–2613, May 1993.

[17] R. Magnusson and S. S. Wang, "New principle for optical filters," *Appl. Phys. Lett.*, vol. 61, no. 9, pp. 1022–1024, Aug. 1992.

[18] E. Popov and L. Mashev, “Dispersion characteristics of multilayer waveguides,” *Opt. Commun.*, vol. 52, no. 6, pp. 393–396, Jan. 1985.
[19] E. Anemogiannis and E. N. Glytsis, “Multilayer waveguides: efficient numerical analysis of general structures,” *J. Light. Technol.*, vol. 10, no. 10, pp. 1344–1351, Oct. 1992.
[20] S. T. Chu, W. P. Huang, and S. K. Chaudhuri, “Simulation and analysis of waveguide based optical integrated circuits,” *Comput. Phys. Commun.*, vol. 68, no. 1, pp. 451–484, Nov. 1991.
[21] C. Grivas, “Optically pumped planar waveguide lasers, Part I: Fundamentals and fabrication techniques,” *Prog. Quantum Electron.*, vol. 35, no. 6, pp. 159–239, Nov. 2011.
[22] N.-H. Sun, J. K. Butler, G. A. Evans, L. Pang, and P. Congdon, “Analysis of grating-assisted directional couplers using the Floquet-Bloch theory,” *J. Light. Technol.*, vol. 15, no. 12, pp. 2301–2315, Dec. 1997.
[23] B. R. Mace and E. Manconi, “Wave motion and dispersion phenomena: Veering, locking and strong coupling effects,” *J. Acoust. Soc. Am.*, vol. 131, no. 2, pp. 1015–1028, 2012.
[24] D. Marcuse, “Directional couplers made of nonidentical asymmetric slabs. Part I: Synchronous couplers,” *J. Light. Technol.*, vol. 5, no. 1, pp. 113–118, 1987.
[25] W.-P. Huang, “Coupled-mode theory for optical waveguides: an overview,” *JOSA A*, vol. 11, no. 3, pp. 963–983, Mar. 1994.
[26] H. A. Haus and W. Huang, “Coupled-mode theory,” *Proc. IEEE*, vol. 79, no. 10, pp. 1505–1518, Oct. 1991.
[27] A. Hardy and W. Streifer, “Coupled mode theory of parallel waveguides,” *J. Light. Technol.*, vol. 3, no. 5, pp. 1135–1146, Oct. 1985.
[28] A. Yariv, “Coupled-mode theory for guided-wave optics,” *IEEE J. Quantum Electron.*, vol. 9, no. 9, pp. 919–933, Sep. 1973.
[29] S. L. Chuang, *Physics of photonic devices*, vol. 80. John Wiley & Sons, 2012.
[30] P. S. J. Russell, “Bloch wave analysis of dispersion and pulse propagation in pure distributed feedback structures,” *J. Mod. Opt.*, vol. 38, no. 8, pp. 1599–1619, 1991.
[31] K. C. Chang, V. Shah, and T. Tamir, “Scattering and guiding of waves by dielectric gratings with arbitrary profiles,” *JOSA*, vol. 70, no. 7, pp. 804–813, 1980.
[32] S. G. Johnson and J. D. Joannopoulos, “Introduction to photonic crystals: Bloch’s theorem, band diagrams, and gaps (but no defects),” *Photonic Cryst. Tutor.*, pp. 1–16, 2003.
[33] K. M. Ho, C. T. Chan, and C. M. Soukoulis, “Existence of a photonic gap in periodic dielectric structures,” *Phys. Rev. Lett.*, vol. 65, no. 25, pp. 3152–3155, Dec. 1990.
[34] “Photonic crystals: putting a new twist on light | Nature.” [Online]. Available: https://www.nature.com/articles/386143a0. [Accessed: 05-Jun-2018].
[35] S. G. Johnson, S. Fan, P. R. Villeneuve, J. D. Joannopoulos, and L. A. Kolodziejski, “Guided modes in photonic crystal slabs,” *Phys. Rev. B*, vol. 60, no. 8, pp. 5751–5758, Aug. 1999.
[36] W. Streifer, D. Scifres, and R. Burnham, “Coupling coefficients for distributed feedback single- and double-heterostructure diode lasers,” *IEEE J. Quantum Electron.*, vol. 11, no. 11, pp. 867–873, Nov. 1975.
[37] A. Yariv and M. Nakamura, “Periodic structures for integrated optics,” *IEEE J. Quantum Electron.*, vol. 13, no. 4, pp. 233–253, 1977.

[38] R. März and H. P. Nolting, “Spectral properties of asymmetrical optical directional couplers with periodic structures,” *Opt. Quantum Electron.*, vol. 19, no. 5, pp. 273–287, 1987.
[39] K. Muhieddine, A. Lupu, E. Cassan, and J.-M. Lourtioz, “Proposal and analysis of narrow band transmission asymmetric directional couplers with Bragg grating induced phase matching,” *Opt. Express*, vol. 18, no. 22, pp. 23183–23195, 2010.
[40] N. Izhaky and A. Hardy, “Analysis of grating-assisted backward coupling employing the unified coupled-mode formalism,” *JOSA A*, vol. 16, no. 6, pp. 1303–1311, 1999.
[41] R. R. A. Syms, “Improved coupled-mode theory for codirectionally and contradirectionally coupled waveguide arrays,” *JOSA A*, vol. 8, no. 7, pp. 1062–1069, 1991.
[42] J. Hong and W. Huang, “Contra-directional coupling in grating-assisted guided-wave devices,” *J. Light. Technol.*, vol. 10, no. 7, pp. 873–881, 1992.
[43] A. A. Hardy, “A unified approach to coupled-mode phenomena,” *IEEE J. Quantum Electron.*, vol. 34, no. 7, pp. 1109–1116, 1998.

Appendix A: TE Fields in Multilayer Structure

This appendix discusses the field components for TE modes in multilayer structures, along with the boundary conditions that they should satisfy. The schematic of a multilayer structure is shown in Figure A.1.

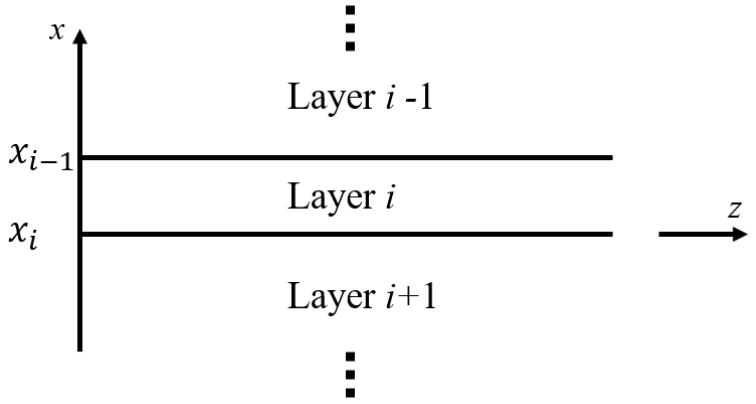

Fig. A. 1 Schematic of a multilayer structure

Each layer of the structure consists of one type of homogeneous dielectric media, and the whole structure is invariant in both the *y*- and *z*-directions. With time dependence in the form of $e^{j\omega t}$, the fields inside the structure satisfy the following Maxwell equations:

$$\nabla \times \vec{E} = -j\omega\mu\vec{H} \tag{A.A.1a}$$

$$\nabla \times \vec{H} = j\omega\varepsilon\vec{E}\,. \tag{A.A.1b}$$

Then we further spatially decompose the field vector and Nabla operator as $\vec{E} = \hat{x}E_x + \hat{y}E_y + \hat{z}E_z$, $\vec{H} = \hat{x}H_x + \hat{y}H_y + \hat{z}H_z$ and $\nabla = \hat{x}\frac{\partial}{\partial x} + \hat{y}\frac{\partial}{\partial y} + \hat{z}\frac{\partial}{\partial z}$, and focus on the scalar components. Then, if we assume fields are propagating along *z*-direction, then $E_z = 0$ for TE polarization; second, from the *y*-invariance of the structure, we can conclude that each

field component is invariant in the y-direction, in other words: $\frac{\partial}{\partial y}E_i = \frac{\partial}{\partial y}H_i = 0$, where $i = x, y, z$. Based on these two findings, we can transform the two vector Maxwell equations into a set of six scalar equations:

$$\begin{cases} \frac{\partial E_y}{\partial z} = -j\omega\mu H_x \\ \frac{\partial E_x}{\partial z} = -j\omega\mu H_y \\ \frac{\partial E_y}{\partial x} = -j\omega\mu H_z \\ \frac{\partial H_y}{\partial z} = j\omega\varepsilon E_x \\ \frac{\partial H_x}{\partial z} - \frac{\partial H_z}{\partial x} = j\omega\varepsilon E_y \\ \frac{\partial H_y}{\partial x} = 0 \end{cases} \tag{A.A.2}$$

Assuming the spatial dependence is $e^{-jk_z z}$, then we can find that $(k_0^2 - k_z^2)E_x = 0$ should always be satisfied for arbitrary k_0 and k_z, where $k_0 = \omega^2\mu\varepsilon$ is the wavenumber in free space. Therefore, we can deduce that $E_x = 0$ and $H_y = 0$ for TE waves in the structure, such that the existing field components are E_y, H_x and H_z. After some calculation, we can further reduce the six equations into two equations, which are:

$$-j\omega\mu H_z = \frac{\partial E_y}{\partial x} \tag{A.A.3a}$$

$$-j\omega\varepsilon E_y - j\frac{1}{\omega\mu}\frac{\partial^2 E_y}{\partial z^2} = \frac{\partial H_z}{\partial x}\,. \tag{A.A.3b}$$

Notice that these two equations can be treated as equivalent Maxwell equations for TE waves in the multilayer structure. Moreover, at each interface between adjacent layers, the tangential components of E and H (E_y, H_z) should be continuous, which is known as the boundary condition. Since the difference of μ among layers is ignored, we conclude that the boundary condition in our scenario is that both E_y and $\frac{\partial E_y}{\partial x}$ are continuous at each interface.

Appendix B: TE Fields in the Grating Region

This appendix discusses the TE fields in the grating layer, along with the boundary conditions that they should satisfy. We started with deriving the boundary conditions for each spatial harmonic. Take the upper boundary $x = x_{k-1}$ as an example. The continuity of $E_{yn}(x)$ and $\frac{\partial E_{yn}(x)}{\partial x}$ are still valid at this boundary, which can be written as:

$$E_{yn}^{(k)}(x_{k-1}) = E_{yn}^{(k-1)}(x_{k-1}) \text{ and } \frac{\partial}{\partial x}\left(E_{yn}^{(k)}(x_{k-1})\right) = \frac{\partial}{\partial x}\left(E_{yn}^{(k-1)}(x_{k-1})\right). \quad \text{(A.B.1)}$$

In (3.3), we already calculated the amplitude coefficients vector $\underline{C}^{(k-1)}$. Therefore, in terms of the field distribution in layer (k-1), the field values at $x = x_{k-1}$ are written as:

$$E_{yn}^{(k-1)}(x_{k-1}) = \left\{s_{n12}\exp\left(jk_{xn}^{(k-1)}x_{k-1}\right) + s_{n22}\exp\left(-jk_{xn}^{(k-1)}x_{k-1}\right)\right\}\cdot b_n^{(1)} \quad \text{(A.B.2.a)}$$

$$\frac{\partial}{\partial x}\left(E_{yn}^{(k-1)}(x_{k-1})\right) = jk_{xn}^{(k-1)}\left\{s_{n12}\exp\left(jk_{xn}^{(k-1)}x_{k-1}\right) - s_{n22}\exp\left(-jk_{xn}^{(k-1)}x_{k-1}\right)\right\}\cdot b_n^{(1)}. \quad \text{(A.B.2.b)}$$

Taking advantage of matrix elements $t_n^{(k-1)}$ of the $\underline{\underline{T}}$ matrix for nth harmonic in layer (k-1), equations (A.B.2) can be written as:

$$E_{yn}^{(k-1)}(x_{k-1}) = (s_{n12}t_{n11}^{(k-1)} + s_{n22}t_{n12}^{(k-1)})\cdot b_n^{(1)} \quad \text{(A.B.3.a)}$$

$$\frac{\partial}{\partial x}\left(E_{yn}^{(k-1)}(x_{k-1})\right) = (s_{n12}t_{n21}^{(k-1)} + s_{n22}t_{n11}^{(k-1)})\cdot b_n^{(1)}. \quad \text{(A.B.3.b)}$$

Inserting (A.B.3) in (A.B.1.) and combining the two equations will lead to:

$$\frac{\partial}{\partial x}\left(E_{yn}^{(k)}(x_{k-1})\right) = \frac{(s_{n12}t_{n21}^{(k-1)}+s_{n22}t_{n11}^{(k-1)})}{(s_{n12}t_{n11}^{(k-1)}+s_{n22}t_{n12}^{(k-1)})}\cdot E_{yn}^{(k)}(x_{k-1}) \quad \text{(A.B.4)}$$

which is the equivalent boundary condition at $x = x_{k-1}$. Similarly, we can derive the equivalent boundary condition for each spatial harmonic at $x = x_k$ as:

$$\frac{\partial}{\partial x}\left(E_{yn}^{(k)}(x_k)\right) = \frac{(r_{n11}m_{n21}^{(k+1)}+r_{n21}m_{n11}^{(k+1)})}{(r_{n11}m_{n11}^{(k+1)}+r_{n21}m_{n12}^{(k+1)})}\cdot E_{yn}^{(k)}(x_k) \quad \text{(A.B.5)}$$

where $m_n^{(k+1)}$ are elements of transfer matrix $\underline{\underline{M}}$ for nth harmonic in layer (k+1).

Next, we will solve the TE fields inside the grating region through the equivalent Maxwell equations given in (3.7), which are:

$$-j\omega\mu H_z^{(k)} = \frac{\partial E_y^{(k)}}{\partial x} \tag{A.B.6.a}$$

$$-j\omega\varepsilon E_y^{(k)} - j\frac{1}{\omega\mu}\frac{\partial^2 E_y^{(k)}}{\partial z^2} = \frac{\partial H_z^{(k)}}{\partial x}. \tag{A.B.6.b}$$

Since in the grating region, the relative dielectric constant $\varepsilon(x,z)$ is periodic along the z-direction, as are both $E_y^{(k)}$ and $H_z^{(k)}$ according to the Floquet-Bloch theorem. We can expand them using Fourier series as:

$$E_y^{(k)}(x,z) = \sum_{n=-\infty}^{\infty} E_{yn}^{(k)}(x)e^{-j(k_{z0}+nK)z} \tag{A.B.7.a}$$

$$H_z^{(k)}(x,z) = \sum_{m=-\infty}^{\infty} H_{zm}^{(k)}(x)e^{-j(k_{z0}+mK)z} \tag{A.B.7.b}$$

$$\varepsilon(x,z) = \sum_{p=-\infty}^{\infty} \varepsilon_n(x)e^{jpKz}. \tag{A.B.7.c}$$

For the future convenience of this derivation, we use n, m, and p to denote the order of each Fourier harmonic respectively. Inserting (A.B.7) into (A.B.6.) will generate two sets of infinite number of equations, which are impossible to be completely solved. In this case, we select a finite number of spatial harmonics, from order $-j_1$ to j_2, to represent the fields. The expanded form of (A.B.6) will be:

$$\sum_{n=-j_1}^{j_2} \frac{\partial E_{yn}^{(k)}(x)}{\partial x} e^{-j(k_{z0}+nK)z} = -j\omega\mu \sum_{m=-j_1}^{j_2} H_{zm}^{(k)}(x)\, e^{-j(k_{z0}+mK)z} \tag{A.B.8.a}$$

$$\sum_{m=-j_1}^{j_2} \frac{\partial H_{zm}^{(k)}(x)}{\partial x} e^{-j(k_{z0}+mK)z}$$

$$= -j\omega\varepsilon_0 \left\{ \sum_{p=-\infty}^{\infty} \sum_{n=-j_1}^{j_2} \varepsilon_p E_{yn}^{(k)}(x) e^{-j(k_{z0}+nK-pK)z} - \sum_{n=-j_1}^{j_2} \frac{k_{zn}^2}{k_0^2} E_{yn}^{(k)}(x) e^{-j(k_{z0}+nK)z} \right\} \tag{A.B.8.b}$$

where $k_0^2 = \omega^2\mu\varepsilon_0$ is the free-space wavenumber, and k_{zn} is the complex propagation constant for nth harmonic. We first focus on (A.B.8.a). Thanks to the orthogonality of the Fourier harmonics, A.B.8.a) is equivalent to a set of linear equations, which are:

$$\frac{\partial E_{yn}^{(k)}(x)}{\partial x} = -j\omega\mu H_{zm}^{(k)}(x)\delta_{mn} \tag{A.B.9}$$

where n and m are from $-j_1$ to j_2. Similarly, the second equation is equivalent to:

$$\frac{\partial H_{zm}^{(k)}(x)}{\partial x} = j\omega\varepsilon_0 \left(\frac{k_{zn}^2}{k_0^2}\delta_{nm} - \varepsilon_{n-m} \right) E_{yn}^{(k)}(x) \,. \tag{A.B.10}$$

If we further define the field vectors for the grating layer as:

$$\underline{E_y}^{(k)}(x) = \left(E_{y,-j_1}^{(k)}(x), \cdots, E_{y,0}^{(k)}(x), \cdots, E_{y,j_2}^{(k)}(x) \right)^T \tag{A.B.11.a}$$

$$\underline{H_z}^{(k)}(x) = \left(H_{z,-j_1}^{(k)}(x), \cdots, H_{z,0}^{(k)}(x), \cdots, H_{z,j_2}^{(k)}(x) \right)^T. \tag{A.B.11.b}$$

(A.B.6) can be written in the form of matrix equations like:

$$\frac{\partial}{\partial x}\left(\underline{E_y}^{(k)}(x) \right) = \underline{\underline{Q}} \cdot \underline{H_z}^{(k)}(x) \tag{A.B.12.a}$$

$$\frac{\partial}{\partial x}\left(\underline{H_z}^{(k)}(x) \right) = \underline{\underline{P}} \cdot \underline{E_y}^{(k)}(x) \tag{A.B.12.b}$$

where the matrix elements for $\underline{\underline{Q}}$ and $\underline{\underline{P}}$ are given as:

$$q_{mn} = -j\omega\mu\delta_{mn} \tag{A.B.13.a}$$

$$p_{mn} = j\omega\varepsilon_0 \left(\frac{k_{zn}^2}{k_0^2}\delta_{nm} - \varepsilon_{n-m} \right) \tag{A.B.13.b}$$